

Responses to reviews of “The Alaiz Experiment: untangling multi-scale stratified flows over complex terrain” by Santos et al. wes-2020-89

Pedro Santos

November 2, 2020

We have received three comments and reviews which are addressed in chronological order. All changes in the manuscript are clearly marked in the attached version.

1 Review by anonymous Referee #1

I enjoyed reading the manuscript. It brings up very interesting flow situations from a modern measurement campaign. It is my impression that the scientists behind the study made a great effort compiling data from, and running, such an extensive campaign. In my judgement the study would be improved by clarifying the aim of the study; Is it to present the campaign? Is it to present important flow phenomena, and in that case, why are they important, and why were these two cases selected? Based on the aim of the study, the background could be improved by focusing on the previous research related to the aim. The basis of distinguishing the hydraulic jump from a lee wave could be strengthened, especially with the RASS showing semi-layered structure in the potential temperature. A linear stability analysis could potentially be useful. I think the climatological consequences of the findings could be highlighted more. The assessment of the prevalence of conditions linked to hydraulic jump was interesting, and it would be valuable with something similar also for the layered flow.

Thanks for your comments. The objective of this paper is twofold: introduce the experiment and highlight two flow cases selected from a catalogue of flow patterns of interest, both related to wind energy and mountain meteorology. A more clear statement of these two objectives was made by rephrasing a sentence in the introduction, P. 3 L. 21–22.

The distinction between the hydraulic jump and lee-wave activity was based on the Fr number transition combined with the multi-lidar observations, from which we have identified characteristics of a hydraulic-jump-type rotor, i.e., a downslope wind separation at the valley floor and a downstream rotor extending beyond the mountaintop level. We have clarified this discussion in the paragraph stating on P.14 L.32. Yet, the layered flow case was identified mainly through the multi-lidar observations. A statistical assessment of such flow pattern could be performed applying tools such as self-organizing maps to the lidar scans, which go beyond the scope of this work.

Abstract L. 2. Although not necessary, temporal information is also interesting.

The temporal information is not mentioned since the acquisition frequency of the measurement equipment is many times larger than the time scale of the flow patterns. We have clarified this in the abstract.

Abstract L.4 For which of the cases, both? That is not clear at this point.

Yes, it is for both flow cases indeed. We have clarified the sentence.

Abstract L.5. Here the reader does not yet know that you are referring to one of your two cases and that the reference to other cases is interesting in terms of similarity.

We have clarified the sentence specifying that the Froude number analysis is related to the hydraulic jump case.

Abstract. L.9 Perhaps add something on why you think it is well captured by the lidars. So far the reader has only been introduced to the lidar measurements (no other measurements), which means that the flow disconnect could potentially be a measurement problem.

We have clarified the sentence mentioning other ground-based observations.

Introduction L1. Does this refer to climatological or time series? For climatological, what is the basis for saying 4% is low? I understand it may be low compared to historical perspective, but in terms of economy it is perhaps not such a low uncertainty

It refers to the climatological mean. The 4% is mentioned as low in a historical perspective. We have clarified the sentence with reference to points mentioned by the reviewer.

P1. L.15. Additional suitable references for this claim. For example Ayotte 2008 for micro scale models, recent work on validation for the NEWA model (perhaps Drenkämper 2020). In terms of analytical work there are also investigations into this by Finnigan and Belcher (2004), and perhaps also the original theory for flow over hill by Hunt.

We have rephrased the sentence with a more quantitative claim referencing the NEWA validation paper by Dörenkämper et al., as suggested.

P1. L.20 As far as I remember the cited literature does not give a summary of the available validation data. I do not so much argue with the claim, but I'm not convinced the cited literature really backs up the claim. In fact, due to the NEWA project, there are quite a few data-sets being produced, so perhaps new data-sets are not so rare anymore. I do think the cited literature provides a good reference for the need of validation data.

This paper has the goal of presenting the Alaiz experiment, which is in fact the last full-scale NEWA experiment. Therefore, it aims to fill a gap of high-quality datasets with multiple ground-based observations in complex terrain. We have replaced the word “rare” to “scarce” and added Mann et al. (2017) as a complementary reference.

P2. L.16. Please be specific when referring to new insights.

We have rephrased the sentence stating the objectives of the referenced studies.

P2. L34 For sure, with such a steep a profile, a linear model is bound be somewhat inaccurate. However, as far as I remember, the performance of the non-linear models was not altogether convincing, which might also be worth mentioning.

We agree and we have rephrased the sentence pointing to the biases of non-linear results.

P2. L34. As far as I recall, the Bechmann et al (2011) only used neutral conditions. Are you referring to Berg et al. (2011)? In that case variation in flow pattern or something similar might be better, since I don't think there were any flow model validation in that study, and hence errors might be misleading

Yes, this claims refers to Berg et al. (2011). We have rephrased the sentence accordingly and added the reference for clarity.

P4. L4. Is there a reference for the airborne laser scans?

Yes, we have added a reference from the experiment's dataset.

P5 L.16. I don't think only WLS70 is enough information to characterize the lidar. Consider also including the brand name.

We agree and we have added details of the manufacturer.

P5 L.24 I suppose the availability of the WLS70 is also interesting if it is reported for the tower. Tower width and boom lengths are good to report in my view, as they provide good indication on flow distortion magnitude. Also, data acquisition rates and averaging periods are good to report here if they are not reported further down the text.

These information are stated in the experiment campaign & data report (Cantero et al., 2019), now referenced in the beginning of the section as suggested by the reviewer in the comment below.

P6. L2. What type of sonic? And also same as above. Boom length and tower widths are potentially interesting.

Brand and model of the sonic anemometers are now stated. Further information is in the experiment campaign & data report.

P6. L.13. Reference for the RASS system is missing.

Details of the manufacturer are now included.

P7. L3. Consider moving this reference to the beginning of the instrumentation section.

We have moved as suggested, since we agree that the reference to the experiment campaign & data report in the beginning of the section will be helpful for the reader that wishes to directly have a more detailed description of the instrumentation.

P7 L10. Consider also mentioning what maximum dz difference this implies. On the other hand, I suppose also errors in the azimuth angle are interesting.

We have complemented the sentence with the azimuth and elevation error at a reference line-of-sight distance of 4000 m. Both azimuth and elevation pointing errors are stated in the referenced table.

P8 L10. From this I take it you first average the radial wind speeds and then compute horizontal vectors? This could be clarified in the beginning of the paragraph, as I suppose the option of calculating horizontal wind vectors and then averaging also exist. The earlier mentioning synchronization makes it a bit unclear.

No, the RHI scans are superimposed meaning that each one depicts radial wind speeds, i.e., along the laser beam. The coplanar RHI scans give the possibility to reconstruct the wind vector projected onto the transects plane within the overlapping region of both scans, in the middle of the valley. Here, we choose only to superimpose the scans since the studied flow phenomena happens in a spatial scale that covers the entire scanning area.

P10 L6. "Can represent the wind climate" is perhaps a bit general. I see what the authors mean, but on the other hand even 8 years leave room for some uncertainty regarding the true wind climate (in terms of for example the true long term average wind speed). In terms of containing a representative set of meteorological conditions I agree with the authors.

We agree that the claim is overstated and we have rephrase it accordingly.

P10 l.14 As in 20% of the slopes higher than 16.7%?

The sentence was rephrased for clarity.

P10, final line: Which is defined here as ...

Ok, modified.

P11 L11. The reference height of 10 m is rather low for the scales of this paper, I suppose? The scales in Berg et al (2011) were much smaller. This means the stratification at levels relevant to wind turbines will generally be much stronger, since those heights are a magnitude larger. I think it is useful also to use 10 m, but some discussion might be warranted. Did the authors try to use Ri number from the RASS to assess large scale stratification?

We have performed a complementary analysis using a gradient Richardson number, where the potential temperature gradient has been taken from the RASS and the wind shear computed using multiple heights as in Högström (1988), but with a higher-order polynomial. This analysis gave similar results in terms of distribution of stability classes as well as mean vertical wind speed profiles. We have added a sentence stating that this analysis was performed.

P11 L15. Are the wind speeds also at 10 m height? The same point as above could be made here as well. One could argue that for wind turbine applications the dependence of wind speed with stratification should be representative for turbine heights. Fig. 7 may give the impression that for higher wind speeds it is almost exclusively neutral conditions, while for wind turbine relevant heights the situation might be different.

We agree that the usage of Obukhov length close to the surface is representative to a limited size of eddies in the atmosphere. However, the objective of section 3.2 was to solely present a picture of the distribution of wind conditions in terms of stratification at the valley center. For the stratified periods where the selected large-scale flow patterns are studied we have chosen to use the Froude number.

Figure 7. Since the experiment was in Spain, it might be good to mention what time is referred to for the x-axis. Local (sun) time, local (Spain) time, or UTC? Why does NU come before U?

The time is in UTC and this information was added in the caption. The legend with stability classes was corrected.

Figure 8. In my opinion the figure would be improved by adding confidence bounds and possibly lines connecting the dots. It would also be valuable to know the filtering criteria for the averaging, or at least which period that is used.

We agree and Figure 8 was redone, with shaded areas denoting associated errors of the mean. The normalized mean profiles represent the entire extensive measurement period, hence in the text we have also added the number of 30-min profiles considered for each analyzed sector.

P.11 L26 Move this to P13 l 10, or move what is there up here (what you use as reference temperature).

Agreed and the sentences were rearranged.

P13. L15. Reference for this statement? I rather thought of a hydraulic jump as a continuity phenomenon (including a transition to turbulence, linked to the lower velocity), with subsequent increase of potential energy. But I'm not that familiar with theory. I guess I object to that the atmosphere "wants" to recover potential energy.

Kaimal and Finningan (1994) state "The basic categories of supercritical flow (where the inversion rises over the hilltop) and subcritical flow (where it drops) as well as the possibility of hydraulic jumps, the abrupt, turbulent transitions from one state to another [...]". We have replaced the word "discontinuity" to "abrupt and turbulent transition" for clarity and added this reference.

Figure 9, and accompanying discussion. Do you have any criteria for distinguishing a hydraulic jump from a regular lee wave? The finite length of the low velocity region behind the jump in Fig. 9 (particularly in panel 2) makes it look to me also a bit like a wave (also the shape of the jet in panel 1).

The characterization of the hydraulic jump in this work is based on: (i) the observed supercritical to subcritical transition, (ii) lidar measurements showing that the downslope flow separation occurs at the valley floor and (iii) the lidar-observed rotor downstream extends beyond the mountaintop level. However, we acknowledge that towards the end of the period these flow features are no longer observed and the observations tend to evidence a lee-wave-type rotor. We have made this clear in the text.

Fig. 10. Confidence bounds (even if estimated) would help the argument made in the text (that the Froude number really decreases at MP5).

We do not see how to estimate such confidence bounds. Instead, we have added a sentence discussing the intrinsic variability of the Froude computation in this study (P. 13 L. 9–11), which do not necessarily represent the entire inversion depth. Furthermore, the decrease in Fr number is connected to the change in flow behavior to a lee-wave-type rotor, as shown by the multi-lidar measurements.

P15. L18. Horizontal scale?

Agreed and rephrased.

Fig. 12. Did you identify the cause of the layers with reverse (negative) wind speed? It is interesting to me that they are on the downstream mountain side. Is it drainage currents from the mountain side?

During this case, the northern general wind is channelized along the Elorz valley generating a westerly flow. As the evening advances and the surface thermal inversion grows, this western flow takes either a more northern (blue color) or southern (red) component depending on the location within the valley atmosphere. The red areas in Figure 12 indicate those locations of the valley where the flow has a southwesterly direction, mainly located at the valley center and over the southern slope. The cause for this wind direction could not be fully identified. It could either have a dynamic origin (i.e. the stably stratified flow enters into the valley with a northwesterly direction and turns into a southwesterly direction after impacting over the southern slopes of the valley) or be the result of a westerly wind merged with a southern drainage flow generated over the mountain southern slopes.

P18 L5. I think in order to say that this study presents the Alaiz experiment, there should be more substance regarding the experimental details. Perhaps introduces is a better word. Also, I think focusing on the flow patterns is interesting enough.

We agree and the first sentence of the conclusions section was rephrased.

Technical comments *The tempus change throughout the text.*

We believe this is good practice in scientific writing. Events that occurred in the past should be described in the past tense. See <https://www.nature.com/scitable/topicpage/effective-writing-13815989/> for further explanation. For example, Section 2 contains a description of the experiment execution (past tense) whereas sections 3 and 4 show results of this study (present tense).

2 Comment by B. Adler

In their introduction, the authors provide a nice overview of recent campaigns focusing on flow features in complex terrain categorized after domain size and slope gradient. However, we think that they missed several recent relevant measurement campaigns siting in the center part of their diagram in Fig. 1. We encourage the authors to consider including these campaigns to complement their overview. One is the PIANO campaign which took place in the Inn Valley over Innsbruck in Austria in 2017 focusing on cold pool and foehn interactions (Haid et al., 2020). Several scanning Doppler lidars were deployed in a complex scanning configuration consisting of coplanar RHI and PPI scans as well as vertical stare mode to get insight into the mean and turbulent structure of the three-dimensional flow. Recent coplanar Doppler lidar measurements were conducted in the complex topography around the city of Stuttgart in south-western Germany focusing on mesoscale flow structures and convective cells (Adler et al. 2020). In 2019, a set of six Doppler lidars was deployed about 20 km east of Innsbruck in the Inn Valley to study the three-dimensional flow structure in the valley under different synoptic conditions. Three of the lidars performed synchronized coplanar RHI scans to capture the cross-valley kinematic flow structure across the whole valley. A BAMS paper about the campaign and measurements is currently under review (Adler et al. 2020). Some information on the campaign were presented during the 19th Conference on Mountain Meteorology and on the KIT website.

We thank you for the comment. We were not aware of these mentioned campaigns in the Inn Valley involving multi-lidar measurements. Therefore, we have decided to modify Figure 1 and include an insert with the Inn Valley area that covers both the PIANO and CROSSINN experiments. We have also added a reference of each experiment in the Introduction.

3 Review by anonymous Referee #2

This study presents measurements from a recent field campaign in the Alaiz mountains, northern Spain. A range of sophisticated equipment, including wind profilers, sonic anemometers and masts for measuring wind and temperature profiles, is employed to probe the flow in transects across a valley between two mountain ridges. These measurements are used to characterize two flow regimes (a hydraulic jump and a valley flow stagnation situation) for orography whose combination of horizontal scale and steepness fills a gap hitherto relatively unexplored by previous field campaigns. Consisting of an essentially observational

study, containing a large amount of original results, relevant for both better understanding orographic flows and the requirements for their accurate numerical modelling, this manuscript is relevant and appropriate to Wind Energy Science. The research seems sound and the manuscript is well written and well organized. My main objection, which is nevertheless minor and will be detailed below, concerns application of known theoretical insights, developed for idealized flows, to the measured hydraulic jump. I think that the paper should be acceptable for publication after minor revisions.

Main point: Use of the Froude number to diagnose super-critical or sub-critical flow, and therefore the occurrence of a hydraulic jump, is one of the most questionable aspects of the results presented. It is tricky to apply concepts developed for idealized cases to realistic conditions, but it must be recognized that by suitably choosing either the definition of Fr or values of the parameters included in it, Fr may vary within a wide range. D is defined as 500 m, based on the elevation difference between MP5 and M7. This seems a bit arbitrary, since D is defined by Rotunno and Lehner (2016) as the depth of a stratified layer and, for example, in Figs. 11 and 12 the atmospheric layer with stronger stratification seems much shallower. It makes more sense to equate D with the layer of high wind speed from the lidar measurements (as the authors do), but the connection with stratification still needs to be clarified. It is mentioned that the potential temperature gradient used to calculate the N included in Fr is obtained by linear interpolation between measurements at 2 and 80 m or 2 and 113 m, but this depth is much smaller than 500 m, so this value of N cannot be considered representative of the stratified layer D . I could not find any allusion to how the value of U included in Fr is estimated. All of these aspects need to be justified in a physically more convincing way, as the estimated value of Fr is very sensitive to them.

Firstly, we thank the reviewer for the comments. We agree that using a two-layer flow theory (Long, 1954) to describe a full-scale three dimensional flow has several caveats, as detailed by Strauss et al., 2016. Since the Froude number is an important parameter for the analysis, we have extended the explanation of how it is computed (including the choice for U) and added a discussion of the caveats that emerge as a result of our choices, including the fact that neither U nor N represent the entire inversion depth.

Furthermore, we would like to clarify to the reviewer that the classification of this flow episode relied mostly on the multi-lidar observations. From them, we have identified characteristics of a hydraulic-jump-type rotor, i.e., a downslope wind separation at the valley floor and a downstream rotor extending beyond the mountaintop level. We acknowledge the influence of the Tajonar ridge downstream the mountain and the presence of valley flow with channeling effects dissociate this episode from an idealized rotor assumed by the two-layer model. However, we believe this analysis adds value to the characterization of lee-side atmospheric hydraulic jumps and that the observations bear sufficient similarity to deserve this classification.

Page 1, line 19: "several processes are included in the former but not in the latter" (when referring to meso- and micro-scale models). It would be good to be more specific here by briefly specifying what some of these processes are.

We have rephrased and added specific examples.

Page 3, caption of Figure 1: It should be mentioned in this caption that in the insets the blue colour represents low elevation and yellow represents high ele-

vation. Is the colour scale arbitrary, or does it have some quantitative meaning? It is strange that the orography of T-REX is mostly blue.

The explanation of the color bar of the inserts is now explained in the caption and in the text. The color scale aims to represent the largest elevation changes of each site. Both T-REX and WFIP2 sites were adjusted and a new site (Inn Valley) was added, as suggested above by B. Adler.

Page 4, line 3: "northwestern part of Spain". Given that these mountains are near the Pyrenees, this should be "northeastern" instead, I think.

We have rephrased to "northern part of Spain" instead.

Page 4, caption of Figure 2: "CP" is denoted by light blue, but this colour (without a nearby white colour for comparison) looks rather white instead. Consider using a different colour, or a different description (but this is just a suggestion).

The image is in high quality, so one can zoom in and distinguish the colors.

Page 6, line 9: "hectometer scale". If I am not mistaken, a hectometer is 100 m. It would perhaps be easier for the reader to understand if this was phrased as "100 m" instead of "hectometer".

The expression of 'hectometer scale' refers to 'the scale of 100 m', as the reviewer points out. Thus, we do not see the need of changing it.

Page 7, line 24: "equally distributed". "equally spaced" might be a more precise description.

Agreed and modified.

Page 8, line 9: "(see figure 4)". It seems to me that the technical aspects about the RHI scan that are discussed in this passage are somewhat unrelated to the aspects that are depicted in Figure 4. Consider whether it makes sense to cite that figure here

The objective of this reference is to direct the reader to the essential part of the experimental setup which is actually used and analyzed in this study.

Page 8, line 14: "staring at M7's 80 m 3D sonic storing". Although I am unfamiliar with the terminology of field work, I wonder if the word "staring" is the most technically accurate one in this context. Please check

We have replaced "staring" with "aiming".

Page 9, Figure 5: In the description of this figure within the text, information should be included on what the angular interval is for calculating the histograms that make up these wind roses. It should also be mentioned in the caption what the percentages labelling the dotted circles mean.

The caption of Figure 5 was complemented with the suggested descriptive details.

Page 9, lines 12-15: "the wind rose measured at the valley floor" is described. Above, when the measurements at the mountain top are described, a turbulence intensity of 7% is mentioned (line 6). If possible, the authors should say what the turbulence intensity in the valley floor measurements is.

We added a sentence stating the average turbulence intensity at 15 m s^{-1} observed from M5 at the valley floor.

Page 10, lines 4-5: "Results show that the NEWA-WRF simulations underestimate the mean wind by more than 1.5 m/s, which is indicative of unresolved speed-up effects in the meso-scale model" (a similar comment is made in page 19, lines 4-6). Do the authors believe that this underestimation is simply caused by insufficient resolution, or are there other factors at play?

The manuscript does not aim to identify the origins of wind speed biases between NEWA-WRF and observations at the mountain top. We are aware of a further analysis at Alaiz using WRF with a horizontal resolution of 1 km in which the mean wind speed bias at the mountain top is improved, but other factors, e.g., synoptic effects from ERA5 not corrected by WRF, cannot be ruled out. Furthermore, Dörenkämper et al. (in press) argue that NEWA-WRF’s “mean wind speed biases are not systematically associated with mischaracterisation of the effective surface roughness or of internal boundary layer effects”.

Page 12, Figure 7: I am puzzled by the order in which the stability categories "nu" and "u" appear in the graphs. It would be natural to expect a sequence "u-nu-n-n-s" in order of increasing stability, but it is "nu-u-n-n-s" instead. Why is that? If this was a mistake, please consider correcting it (although this, of course, does not affect the correctness of the results).

The legend was corrected.

Page 13, line 5: "Fr = pi U/2 N D". I am aware of the fact that the authors define the Froude number based on Rotunno and Lehner (2016), but it would be good to briefly explain the presence of the factor pi/2 in this definition

Done.

Page 13, lines 15-16: The description of the hydraulic jump could be improved. It should be mentioned that the discontinuity that corresponds to the hydraulic jump occurs as a downstream consequence of the flow transition between subcritical and supercritical over the mountain, associated with a downslope windstorm. Perhaps a reordering of the text would do the job, since in lines 18-19 below high amplitude mountain waves and downslope flow are mentioned, and in lines 21-22, supercritical and subcritical flow regimes are mentioned

We have reordered one sentence in the paragraph to highlight the hydraulic jump connection with a downslope flow in the lee side of the mountain. The further explanation of supercritical to subcritical flow transition remained in the second paragraph since we consider it needs a proper reference and explanation, in connection with the Froude number, for the wind energy community readers that might not be familiar with such concepts.

Page 13, lines 17-18: "It differs from atmospheric gravity waves or lee waves since it involves a discontinuity and requires nonlinear dynamics to be described". Some gravity waves and lee waves also require nonlinear dynamics to be described. It is just that the nonlinearity of hydraulic jumps is more extreme

Agreed. We have rephrased the sentence to clarify that the hydraulic jump discontinuity is stronger.

Page 13, lines 23-24: The authors refer here to solutions that use "a Fr scaled with the maximum wave speed given by (g D)^(1/2)". Clearly this is different from the Froude number defined previously and used in the present study. How do the conditions in which this alternative Fr apply differ from those considered in the present study?

The Fr number computation of this study is based on observations up to 80 m above ground from meteorological masts, therefore they are local and do not necessarily represent the entire stratified layer. We have clarified such caveats in the end of section 3. The scaling using $\sqrt{g'D}$, where g' is a reduced gravitational acceleration, could also be applied here if we were able to compute atmospheric variables throughout the boundary layer, e.g., using outputs from numerical simulations.

Page 13, line 30: "We defined $D \approx H \approx 500$ m in section 3.2, which agrees with previous studies". Unless the flow is the same, it is irrelevant whether this value agrees with previous studies or not, since the height of the stable layer, or whatever is used to estimate D , varies between different flows

The mentioned study also assessed the Froude number at the MP5 location, however we agree with the reviewer in the sense that the selection of D is arbitrary. Therefore, we have removed the reference and rephrased the sentence accordingly.

Page 15, lines 3-4: "Fr at MP5 decreases from 1.5 to 1.2 and the M2 measurements evidence a recirculation zone in the lee-side of the mountain". This recirculation zone is usually called a rotor, and it would be worth mentioning that term, perhaps in connection to citation of one or two studies that address that flow structure.

We have rephrased the sentence mentioning that, towards the end of the episode, M2 is located at the bottom of the hydraulic jump rotor, where reverse surface winds are observed. The observations made by Strauss et al. (2016) during the T-REX experiment are referenced here.

Page 15, line 13: "quiescent easterly winds". "Quiescent" is often reserved for situations of calm. Do you mean to say that the easterly winds are "weak", perhaps?

Agreed. 'Quiescent' has been changed into 'weak'.

Page 15, lines 14-15: "The potential temperature profiles (Figure 11c) from S1, M5 and sodar RASS agree and show a stable boundary layer". What is the height of this boundary layer? What is its relation (if any) with the height of the so-called "stable layer".

In this section we were not intended to analyse the boundary layer height and its relation with the temperature profile within the valley. The expression of a "stable boundary layer" was used here to emphasize that the thermal inversion depicted in figure 11c indicates the presence of a stably stratified layer over the valley floor. Since this emphasis may confuse some readers, we have modified it with a more precise description: "The potential temperature profiles (Figure 11c) from S1, M5 and sodar RASS agree and show a thermal inversion".

Page 16, inset in Figures 11(a), and page 18, inset of Figure 13(a): These insets (containing the legends for the 2m wind speed, 2m temperature and temperature difference between 2 m and 0.36 m need to be described in the caption
Done.

Page 16, lines 5-6: "heterogeneous land cover, which causes unequal heat fluxes". How important is this effect compared with orographic effects (causing katabatic and anabatic circulations)?

Both 'mountainous terrain' and 'heterogeneous land cover' are equally important. We have slightly modified the sentence to explicitly mention both effects.

Page 17, line 8: "Both layers are stably stratified, although with different intensity". Curiously, the apparently katabatic flow shown in Figure 12 extends over a substantially higher depth than the more intensely stably stratified layer in the theta profile. Is there an explanation for this?

During this study case, the northern general wind is channelized along the Elorz valley generating a westerly flow. Two clear stages characterise this night: 1) a moderate general wind that interacts with the valley atmosphere until

midnight and 2) the decoupling between the valley atmosphere and the overlying flow as it diminishes intensity after midnight.

These two distinct stages are described in paragraph 3-4 and 5, respectively. Thus, the different stable layers mentioned in paragraph 3 correspond approximately to the red and blue bands that appear in the cross sections of 22:10Z and 00:10Z in figure 12a. We agree that the red band grows vertically covering a great part of the less stable layer at 03:10Z. We believe that this is due to the decoupling between the valley atmosphere and the general wind, as explicitly mentioned in paragraph 5 of this section.

Therefore, for clarification, we have included the times of the RHI scans that we refer to in paragraph 3.

Finally, we'd like to clarify to the reviewer that the red areas in Figure 12 indicate those locations of the valley where the flow has a southwesterly direction, mainly located at the valley center and over the southern slope. The cause for this wind direction could not be fully identified. It could either have a dynamic origin (i.e. the stably stratified flow enters into the valley with a northwesterly direction and turns into a southwesterly direction after impacting over the southern slopes of the valley) or be the result of a westerly wind merged with a southern drainage flow generated over the mountain southern slopes. In any case, this wind dynamics occurs above the stronger thermal inversion developed over the valley floor after midnight. Other works have reported the existence of drainage flows generated over sloping surfaces that flow over the coldest air accumulated at the bottom of the valley (Cuxart et al. 2007, Martínez and Cuxart, 2009).

Page 17, line 12: "The S7 and S9 positions show a recirculation zone". Does this correspond to pooling of the flow? If yes, it would be worth mentioning this explicitly, since cold air pools in valleys are an active area of research.

We agree that cold air pooling in valleys is a very interesting and active area of research. The weak wind speeds observed in S7 and S9 can be explained due to the sheltering effect of the northern mountain range, favouring a strong thermal inversion at the skin level. Thus, 'recirculation zone' has been replaced by 'sheltered zone'. However, we do not feel appropriate to include the 'cold air pool' concept here because these stations are located over the mountain slope (S9) and at the foothills (S7). Nevertheless, the formation of a cold air pool over the valley floor after midnight is explicitly mentioned in the last paragraph of this section.

Page 18, line 2: "An elevated thermal inversion around 720 m asl". It would be good to refer back to Figure 12(b) at this point, so that readers can understand what is being discussed

Done.

Page 18, lines 3-4: "depth of the red band within the valley observed in the RHI scan of 3:10Z". Again, it would be useful to the reader if the authors referred back to Figure 12(a), where this feature can be identified

Done.

Page 18, lines 11-12: "ALEX17 yet poses a further challenge in numerical modeling efforts for its large domain size". I suggest replacing the word "for" in this sentence by "because of"

Agreed and sentence was rephrased.

Page 18, line 14: "wind direction offsets up to 90°". I suggest replacing this passage by "the wind rotates by up to 90°"

Agreed and sentence was rephrased.

Page 19, lines 1-2: I suggest that the reference at the end of the sentence spanning these two lines is moved to after "experimental report", since it seems to refer to that report.

Agreed and reference was moved.

Page 19, lines 13-14: "On the other hand, during stratified conditions with lower wind speeds, valley winds become decoupled from the mountain flow aloft due to thermal stratification". This should be connected to cold-air pooling and valley inversions, and one or two relevant references on these topics should be added

An explicit mention to the formation of a cold air pool, together with a couple of references, has been added into the sentence.

Page 19, line 17: "in terms of its physical description". "its" should be replaced by "their", since the word it refers to, "flows", is plural

Agreed and sentence was rephrased.

Page 19, line 18: "i.a.". I interpret this as meaning "inter alia". Is this abbreviation standard? If not, write it in full form instead.

Yes, it stands for "inter alia" and we consider understandable for the reader without the full form.

Page 19: The "Author contributions" and "Competing interests" sections seem to be in the wrong place, between the Appendix title and its content. They should probably come, either before the Appendix title, or after the Appendix

The sections were rearranged.

Page 21, line 22: Please check if the volume number is correct, as it appears to coincide with the year (2020).

The reference was updated.

Page 22, line 8: "pp. 1-33". I believe the "pp." is unnecessary. Consider removing it.

The reference was updated.

Page 22, line 27: The page range appears to be missing from this reference.

The reference was corrected.

Page 23, lines 21-22: This reference has no volume number or page range.

This reference represents a dataset.

Page 24, line 6: This reference has no volume number or page range.

The reference was corrected.

The Alaiz Experiment: untangling multi-scale stratified flows over complex terrain

Pedro Santos¹, Jakob Mann¹, Nikola Vasiljević¹, Elena Cantero², Javier Sanz Rodrigo², Fernando Borbón², Daniel Martínez-Villagrasa³, Belén Martí³, and Joan Cuxart³

¹Technical University of Denmark, DTU Wind Energy, Risø Campus, Roskilde, Denmark

²National Renewable Energy Centre (CENER), Sarriguren, Spain

³Physics Department, University of the Balearic Islands (UIB), Mallorca, Spain

Correspondence: Pedro Santos (paas@dtu.dk)

Abstract. We present novel measurements from a field campaign that aims to characterize multi-scale flow patterns, ranging from 0.1 to 10 km [in a time-resolved manner](#), in a mountainous region in Northwestern Spain with a mountain-valley-ridge configuration. We select two flow cases where topographic-flow interactions were measured by five synchronized scanning Doppler wind lidars along a 10-km transect line ~~-, including that includes~~ a cross-section of the valley ~~flow~~. We observed a hydraulic jump in the lee-side of the mountain. ~~The~~ [For this case, the](#) Froude number transition from supercritical (> 1) at the mountain to subcritical (< 1) at the valley is in agreement with previous experiments at a smaller scale. For a one-year period, the measurements show such a transition about 10 % of the time, indicating a possible high occurrence of hydraulic jumps. The second flow case presents valley winds that are decoupled from the northerly flow aloft and show a stratified layered pattern, which is well captured by the lidar scans [and complementary ground-based observations](#). These measurements can aid the evaluation of multi-scale numerical models as well as improving our knowledge with regards to mountain meteorology.

1 Introduction

Over flat and homogeneous terrain, such as areas far offshore, the difference between measured and simulated [climatological](#) mean wind speeds ~~is rather low~~ at wind energy relevant heights ~~-, is~~ in some cases less than 4% (Olsen et al., 2017). [This is historically low although there is still economic value in reducing it even further.](#) However, over complex terrain, with steep slopes and varying land cover, such differences can be ~~more substantial~~ [closer to 10% \(Dörenkämper et al., 2020\) depending on terrain complexity](#), implying large uncertainties on the estimated annual energy production of wind farms. Even small deviations in the terrain description over a given area may result in substantial differences in the simulated flow (Lange et al., 2017).

For the prediction of winds in complex terrain, meso-scale models, typically covering scales down to a kilometer or so, have to be coupled with micro-scale models that cover smaller scales down to meters. Meso- and micro-scale models are fundamentally different in the sense that flow processes that are parameterized in the former are resolved in the latter, while several physical processes, [e.g., cumulus clouds and convective systems](#), are included in the former but not in the latter. The scales that are at the interface of the two models have been dubbed *terra incognita* by Wyngaard (2004) and this experimental

investigation aims to explore some sub-meso-scale physical processes. New datasets from complex terrain experiments with details on flow patterns covering these scales are ~~rare~~ scarce and needed to evaluate and quantify the uncertainty of numerical models (~~Sanz Rodrigo et al., 2017~~) (Mann et al., 2017; Sanz Rodrigo et al., 2017). Apart from wind energy, untangling flow over complex terrain is of general interest for the mountain meteorology community (Serafin et al., 2018).

5 Over the last decades, experimental efforts have been conducted with increasing density of instruments and types of measurement aiming to better understand flow conditions in hilly and mountainous terrain. A well-known experiment was performed at the Askervein Hill, which became the main reference in the development and validation of pioneering analytical and linearized flow models dealing with gently sloping terrain (Salmon et al., 1988; Walmsley and Taylor, 1996). Furthermore, the Cooper's Hill experiment (Coppin et al., 1994) used meteorological masts and sonic anemometers to study the flow over a ridge as a
10 function of atmospheric stability.

In more recent endeavors, Doppler wind lidars and airborne instrumentation have been used to characterize large-scale phenomena over steep hills and mountain ranges. Two examples of such are the terrain-induced rotor experiment (T-REX, Grubišić et al., 2008) and the mountain terrain atmospheric modeling and observations program (MATERHORN, Fernando et al., 2015). T-REX focused on low-level vortices formed downstream of a mountain ridge and MATERHORN was a
15 multidisciplinary initiative to approach large-scale atmospheric phenomena in complex terrain, where two major experimental campaigns studied thermally driven winds with strong synoptic forcing. Back to smaller scales, detailed scanning lidar and turbulence measurements were performed at the escarpment of Bolund (Lange et al., 2016; Berg et al., 2011), which ~~brought new insights into~~ detailed turbulence characteristics under flow-terrain interaction. A blind test followed to compare a wide variety of flow models (Bechmann et al., 2011) and wind tunnel prototypes (Kilpatrick et al., 2016; Conan et al., 2016; Lange
20 et al., 2017).

With an extensive collaboration effort in the pursuit of new insights on wind resource characterization, a range of experiments, both onshore and offshore, were performed within the New European Wind Atlas (NEWA) project to evaluate meso- and micro-scale models (Mann et al., 2017). The experiments made extensive use of a recently developed infrastructure that uses synchronized measurements from multiple lidars, the so-called long-range WindScanner system (Vasiljević et al., 2016).
25 The Kassel experiment, performed at the forested hill Rödeser Berg in Germany, was used to quantify the accuracy in the reconstruction of the wind vector with distinct multi-lidar combinations and the lidar's spatial averaging effect on the turbulence spectra (Pauscher et al., 2016). A methodology for the execution of experiments involving multi-lidars was developed during the double-ridge Perdigão experiment in Portugal (Vasiljević et al., 2017), which is the largest experimental venture in complex terrain to date in terms of density of measurement equipment (Fernando et al., 2019). In parallel to the NEWA
30 project, the second Wind Forecast Improvement Project (WFIP2), also deployed a large array of instruments to cover the area around the Columbia Gorge in the United States (Wilczak et al., 2019). This experiment was also focused on the improvement of meso- and micro-scale coupling methods (Haupt et al., 2019).

The Inn Valley, located close to Innsbruck, Austria, is a site where extensive field campaigns took place to characterize atmospheric processes with regards to mountain meteorology. Recent experiments used multiple wind lidars to obtain flow

[patterns to characterize cold-air pool erosion by downslope mountain winds \(Haid et al., 2020\)](#) as well as [cross-valley circulation cells using coplanar multi-lidar observations \(Adler et al., 2020\)](#).

Figure 1 puts the Alaiz experiment in perspective of these complex terrain experiments by comparing the area covered and steepness of the terrain quantified by the upper 10th percentile of the slopes. [The color in the inserts covers the elevation range of each site.](#) In this context, Askervein can be seen as a departure point that gave rise to experiments in larger areas and steeper slopes.

With a small domain but a steep escarpment, Bolund left the realm of gentle slopes, and hence emphasized the limitations of linearized flow models [and eventual biases of non-linear simulations.](#) Due to the very small scales, neglecting the effects of atmospheric stability did not lead to major ~~errors in Bolund~~ [variations in the flow pattern over Bolund \(Berg et al., 2011\)](#)

. On the other hand, in METCRAX II, scanning lidars captured atmospheric hydraulic jumps and cool pool events inside a meteorite crater in Arizona (Lehner et al., 2016). In Kassel and Perdigão, larger areas were investigated that required the use of long-range WindScanners. Perdigão presents a double-hill configuration, 1.5 km apart, which is dominated by micro-scale effects, such as valley winds and recirculation zones, but is also affected by thermal stratification effects that can lead to internal atmospheric gravity waves under stable conditions (Menke et al., 2019; Palma et al., 2019). T-REX and WFIP2 are mountain range studies, too large to be fully covered by a single set of instruments, still with similar thermally stratified flows presented in this study. [In the extreme of terrain complexity, the Inn Valley area hosted multiple experimental campaigns to cover such an alpine region.](#)

As highlighted by Mann et al. (2017), Alaiz covers the mid-range where both micro-scale and meso-scale effects are prevalent. As shown in Figure 1, Alaiz features similar complexity as Perdigão, but is an order of magnitude larger with influence of topographic features that are 10 km or more apart. The area to cover is still within the range of current commercial wind lidars.

This paper ~~presents~~ [firstly introduces](#) the Alaiz Experiment (ALEX17), which aims to peer into multi-scale flow patterns with mountain-valley interactions. ~~In~~ [Secondly, in](#) this work, we are describing two types of flow cases: a layered-stratified valley flow and a hydraulic jump, characterized with multi-lidar measurements and multiple ground-based observations.

This paper is outlined as follows. In section 2 we describe the experimental layout and detail the measurement equipment. Section 3 describes the site climatology and the atmospheric stability is assessed. In section 4 we characterize and discuss the two selected flow cases. Section 5 summarizes the main findings and promotes this data collection as a tool for further analysis and numerical model evaluation.

2 The ALEX17 experiment

2.1 Site Characterization

ALEX17 took place in the Navarre region, in the ~~northwestern~~ [northern](#) part of Spain. The experimental area encompasses the Alaiz mountain range, a region at 1000 m above the mean sea level (asl) with a wind regime favorable for wind energy applications (Sanz Rodrigo et al., 2013). Figure 2a shows the experimental domain (yellow square) within the Iberian Peninsula

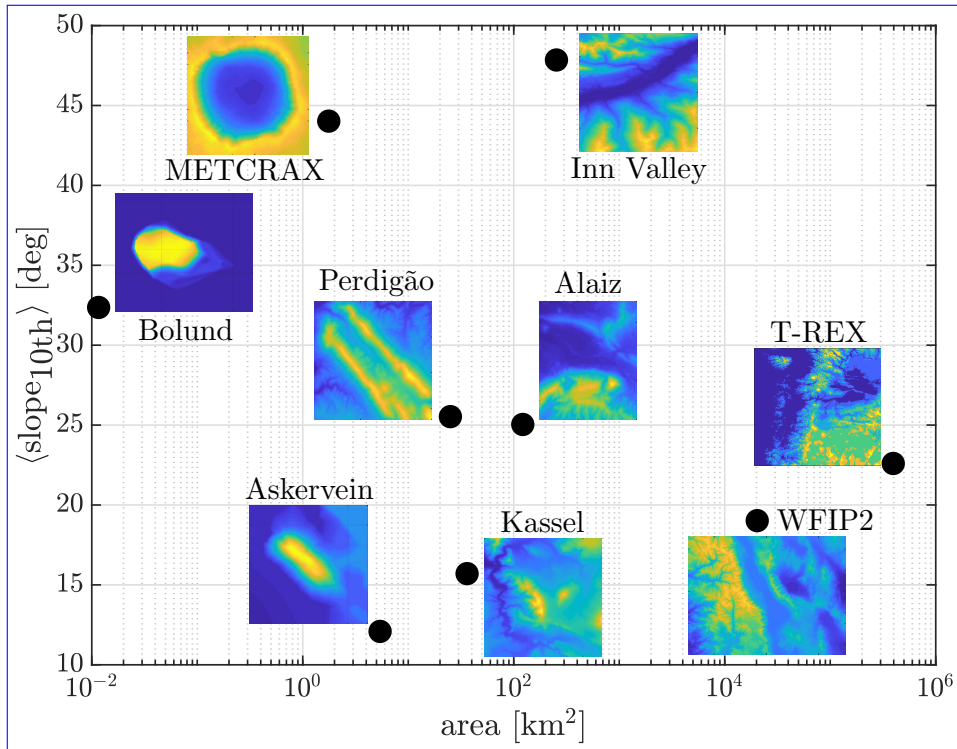


Figure 1. Illustration of the complexity of some atmospheric flow experiments as a function of their area of coverage. The complexity is in terms of the slope: the average 10th percentile of the highest slopes. The inserts besides the markers show contour maps of the relative elevation for each site, [where blue and yellow colors represent low and high elevations, respectively.](#)

with a 1 arcsec resolution elevation map from the Shuttle Radar Topographic Mission (SRTM). The site is situated to the northwest of the Ebro valley, a river basin enclosed by the Pyrenees to the north and the Iberian system to the south.

The large-scale topographical features in the region explain the synoptic forcing present on this site. Jiménez et al. (2013) performed meso-scale modeling with 2-km horizontal resolution over 45 yr and assessed the wind variability over the region.

- 5 Badger et al. (2014) presented a statistical-dynamical downscaling to estimate a generalized wind climate in the same area. Apart from inherent biases between model and observations, both studies showed two main circulation patterns, with northwest (NW) and southeast (SE) flow over the Ebro valley, with a channeling effect caused by an orographic funnel formed by the large-scale features (see figure 2a). The NW circulation is ordinarily called “Cierzo”. Badger et al. (2014) additionally showed that this effect is intensified during stable conditions, where the stratified atmospheric boundary layer (ABL) interacts with the
- 10 orography more actively.

Figure 2b shows the area surrounding the experimental domain with a 2x2-m resolution terrain elevation map based on airborne lidar scans ([Chavez Arroyo, 2019](#)). The Alaiz mountain, to the south, hosts CENER’s wind turbine test site in complex terrain with six test stands (red dots) and a 118-m meteorological mast called MP5 (purple dot). The other test site’s masts (not

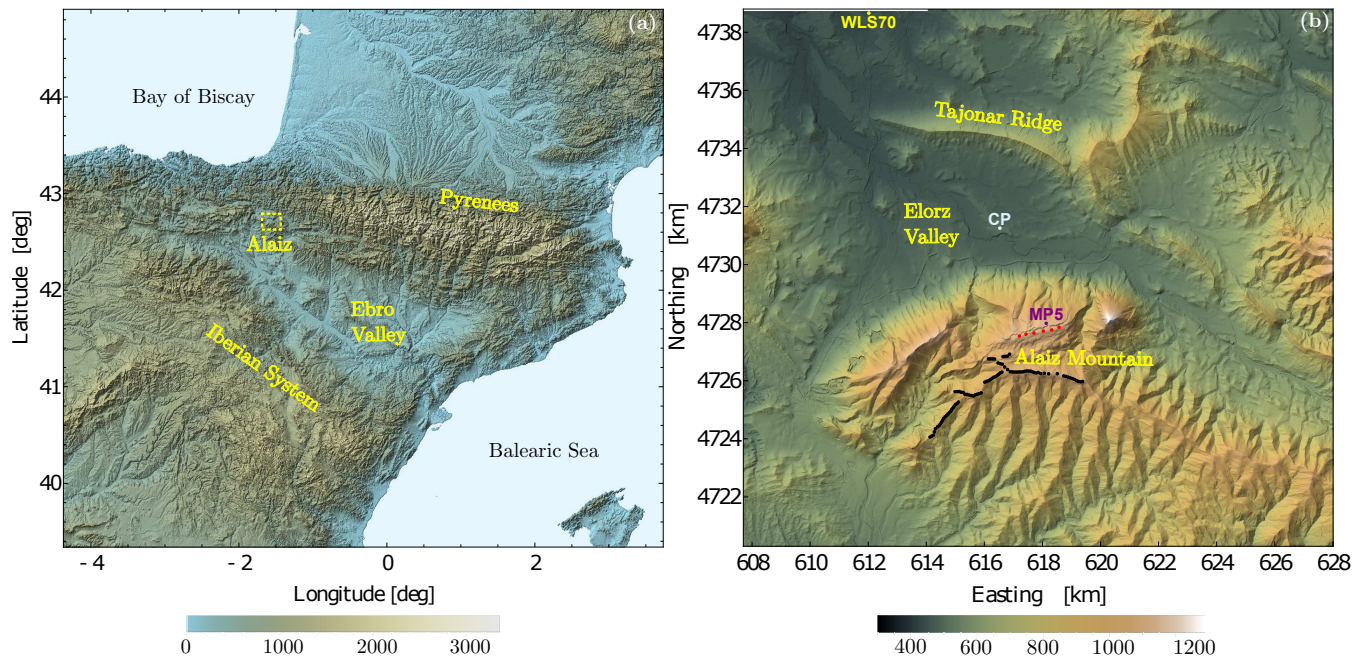


Figure 2. Location and overview of ALEX17. Panel (a) shows the experiment location (yellow rectangle) within the Iberian Peninsula. The experiment is shown in (b), with: CENER’s wind turbine test stands (red) and reference MP5 meteorological mast (purple); Acciona’s wind farms (black); the central position (CP, light blue) and a profiling wind lidar (WLS70, yellow). The colorbars represent the height above mean sea level in meters based on digital elevation models from SRTM (panel a) and lidar aerial scans (panel b) in UTM30 WGS84.

shown) are not part of this experiment. To the south of the mountain plateau, 89 wind turbines (black dots) belong to Acciona’s wind farms called Alaiz and Echagüe, which shows that the site, although challenging, is attractive for wind energy production.

To the north of the Alaiz mountain range, most of the measurement equipment are located at the Elorz valley, 500 m asl, around the central position (CP, blue dot) of the experimental domain. The valley is roughly 10 km wide and 6 km long, bounded by the Tajonar ridge, hereafter called north ridge, which has its peak at 850 m asl. Notice that, as in the large-scale features, the Alaiz mountain and the north ridge are not parallel, also shaping the valley as a funnel. The land cover is heterogeneous (c.f. Figure 4 in Cantero et al., 2019) with villages and distinct kinds of farmland distributed along the valley floor, as well as forest patches on the slopes of the north ridge and the top of Alaiz mountain.

2.2 Timeline and Instrumentation

10 The extensive measurement period (EMP) ran from July 2017 to July 2019, comprising two full years of measurements from the reference mast MP5 and from a long-range profiling wind lidar (WLS70, [Leosphere Inc., Saclay, France](#)) located at the north boundary of the domain (see figure 2b). The Intensive Observational Period (IOP), when all sensors had concurrent measurements, lasted for five months from August 2018 to December 2018.

Figure 3 shows the 100-km² experimental domain, with CP at the center and details of the instrumentation layout. Most instruments were placed in the valley floor, aiming to investigate the topographic interaction on the flow between Alaiz mountain and the north ridge in order to characterize the wind regime at the mountain top, regarded as the region of interest for wind energy. [Cantero et al. \(2019\) documented the ALEX17 campaign, with detailed technical specifications of each of the instruments, together with their geographical coordinates, as well as their operating periods and data availability. Here, we summarize the instruments used in this study.](#)

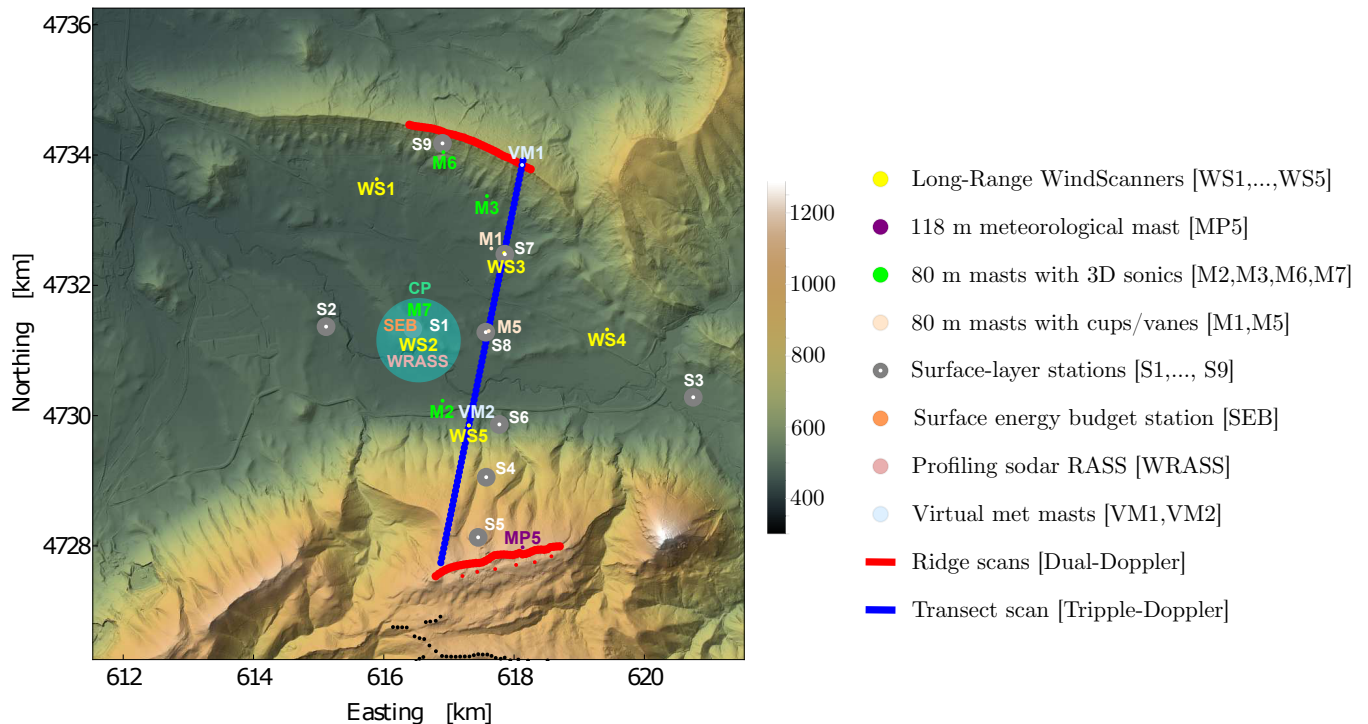


Figure 3. Instrumentation layout of the ALEX17 campaign within the 10 x 10 km experimental domain centered at CP. The legend details each type of measurement station. The transect scan (blue line), detailed in figure 4, is the focus of this study.

Reference meteorological mast (MP5). This is a 118-m meteorological mast located at the mountain top (42°41.7' N, 1°33.5' W). We selected this mast as a reference because it is measuring continuously since 2011 with the same configuration. The wind speed and wind direction data availability at 118 m was 85.4 % between February 2011–January 2019. The mast is equipped with wind and temperature measurements distributed in six main levels: 2, 40, 80, 90, 100 and 118 m above the ground level (agl).

Long-Range WindScanners (WS). Five WindScanner units were distributed along the valley floor, depicted with yellow markers in figure 3. By scanning on vertical planes across the valley, it is possible to visualize the dynamics of multi-scale flow patterns generated by the interaction between the ABL and the topography such as atmospheric waves or flow-separation

regions in the lee side of the ridges. We configured the units to synchronously scan in pairs and triplets, allowing the wind vector reconstruction on top of the ridges and across the valley, shown by red and blue lines in figure 3 and detailed in Sec. 2.3.

Meteorological masts (M). Six 80-m tall meteorological masts were distributed across the valley, marked with distinct colors in figure 3 for masts with either cup/vanes or 3D sonic anemometers. They are located either on the valley floor or in the north ridge slopes. They provide wind speed, wind direction, temperature and turbulent momentum and sensible heat fluxes (for the ones with sonics) profiles at five main levels: 10, 20, 40, 60 and 80 m. In this study, we use ~~3D-Gill WindMaster Pro~~ sonic anemometers and air temperature measurements from M3, M7 and M2, located at the north ridge slope, CP and Alaiz foothills respectively.

Surface-layer stations (S). Due to the heterogeneous land cover, estimation of the horizontal distribution of surface fluxes along the valley and mountain slopes became a need. Nine surface-layer stations, shown with grey markers in figure 3 were deployed for this. Each station had a 2D sonic anemometer at 2 m agl, two levels of temperature (0.36 and 2 m agl) and soil heat flux measurements at a depth of 0.08 m along with soil moisture and temperature at a depth of 0.05 m. These stations were used in a previous study to successfully characterize the spatial variability of atmospheric and soil patterns close to the surface at the hectometer scale (Simó et al., 2019).

Central Position (CP). This is considered a major location of the experiment due to its density of instruments, see figure 3. The CP is located in the middle of the valley, with relative flat surroundings and farmland as the predominant land cover. Apart from WS2 and M7, there were: i) a radar acoustic sounding system, WindRASS ~~-(Scintec AG, Rottenburg, Germany),~~ capable of measuring wind and virtual temperature profiles up to 400 m agl; ii) a surface energy budget (SEB) station, able to estimate the four main components of the surface energy balance (i.e., net radiation, sensible and latent heat fluxes, and ground heat flux). Previous studies in the Ebro valley used the SEB to quantify significant imbalances in the energy budget (Cuxart et al., 2015) and observed the occurrence of low-level jets and katabatic winds with the WindRASS (Cuxart et al., 2012).

~~Cantero et al. (2019) documented the ALEX17 campaign, with further and more detailed technical specifications of each of the instruments, together with their geographical coordinates, as well as their operating periods and data availability.~~

2.3 WindScanner measurements

The planning of ALEX17 WindScanners scanning strategies was built upon the experience of previous experiments (Pauscher et al., 2016; Vasiljević et al., 2017; Menke et al., 2019). ALEX17 used a combination of five long-range wind scanners (LRWS), which can be collocated with a pointing accuracy of up to 0.05 deg and synchronized in time within 10 ms (Vasiljević et al., 2016). The campaign lasted for almost 9 months from May 2018 to January 2019. The pointing error during the IOP was kept within 0.2 deg based on regular hard target mapping (c.f. Table 4 in Cantero et al. (2019)), which represents a deviation of 14 m at a line-of-sight distance of 4000 m.

To execute the ridge, transect and virtual meteorological masts scans shown in figure 3, a total of seven scanning strategies were designed and programmed. With more planned scans than available lidars, each system was scheduled to perform a cycle of three scanning strategies, each lasting 10 minutes, i.e. all trajectories are completed at least twice per hour (four times for the north ridge scan). Table 1 shows the final schedule for each WindScanner.

WindScanner	1 st 10-min interval	2 nd 10-min interval	3 rd 10-min interval
WS1	North ridge scan †	Virtual mast (VM1) ‡	North ridge scan †
WS2	Virtual mast (VM2) ‡	Transect scan †	South ridge scan †
WS3	North ridge scan †	Transect RHI ‡	North ridge scan †
WS4	Virtual mast (VM2) ‡	Transect scan †	South ridge scan †
WS5	Virtual mast (VM2) ‡	Transect RHI + VM1 ‡	Transect RHI ‡

Table 1. Half-hourly repeating schedule of scanning strategies. Scans with † are fully synchronized and those with ‡ start simultaneously at every interval.

The ridge scans, shown as red lines in figure 3, were each composed of 40 evenly distributed points 50-m apart, which followed the terrain profile at 125 m agl. Table 1 shows which pairs of LRWS were programmed to measure synchronously by traversing the beams through the ridgeline points (†), i.e. dual-Doppler measurements. The virtual meteorological masts were defined by the intersection of range-height indicator (RHI) scans. VM1 extended up to 1400 m agl and was measured with WS1 and WS5 during the 2nd interval, whereas VM2 went up to 1200 m agl and consisted of three RHI scans performed by WS2, WS4 and WS5 (triple-Doppler). The RHIs were coordinated, i.e. not fully synchronized ‡, with the laser beams not visiting the same points of the virtual mast at the exact same time.

Figure 4 shows a cross-section of the transect scan, defined by the vertical plane spanned by WS3 and WS5. The transect scan (blue dots) followed the terrain profile (grey area) at 125-m agl. The scan is measured synchronously by WS2 and WS4 at 85 equally distributed spaced points 50-m apart, starting at the north ridge (location of VM1, light blue markers) and ends at the top of the Alaiz mountain, where it met the westernmost point of the south ridge scan. Two overlapping RHIs with opening angles of 15° and 20°, respectively, extend the scan curve upward. See table A1 for further details of these RHI scans.

All RHIs had a range of 5 km, but valid measurements are dependent on data filtering criteria that disregard regions e.g. with low clouds and fog, especially near the Alaiz mountain ridge. Measurements from some meteorological masts are here used to explain flow patterns measured by the RHIs. Hence, the positions of M3, M7, M5, M2 and MP5 were projected onto the transect plane as reference (black dots).

Each RHI scan in figure 4 took ≈ 30 s, so we ensemble-average 20 scans per 10-min period, computed twice every hour. Before averaging a scan, two noise filters are applied: i) a hard target filter, which finds range gates with carrier-to-noise ratio (CNR) larger or equal to 5 dB and removes all range gates beyond this point (see figure 4) and ii) the variation of the radial velocity v_r between consecutive range gates along each line-of-sight (LOS) is estimated to filter out values larger than 1.5 ms^{-1} .

This multi-lidar scanning patterns provided 2D and 3D wind reconstruction over the ridge scans (red lines) and transect scan (blue line), respectively. The combined Z-shaped transect (figure 3) had a length of 10 km and is a unique feature of this experiment. Additionally, after the IOP all systems performed a one-month campaign staring-aiming at M7's 80-m 3D sonic

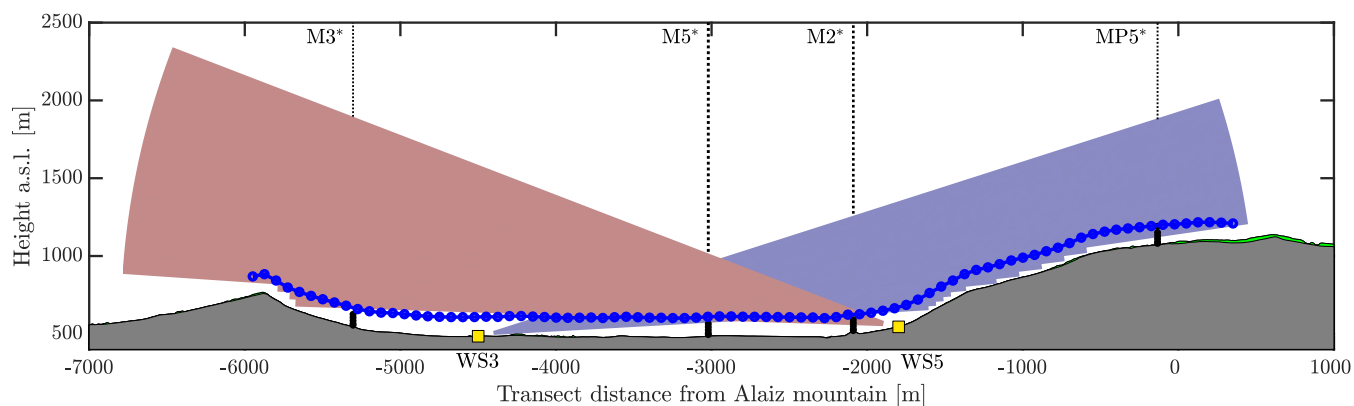


Figure 4. Transect scan on the vertical plane spanned by WS3 and WS5 (yellow squares). Shaded areas represent the superimposed RHI scans after a hard target filtering. The blue dots show the transect scan measured by WS2 and WS4 (out of the plane). The black dots indicate the positions of the masts M3, ~~M7~~M5, M2 and MP5 when projected onto the transect's plane.

~~storing and storing~~, in addition to the wind speeds~~also~~, the raw Doppler spectra. The Z-shaped transect's UTM coordinates can be found in the Supplement.

3 Site wind conditions

3.1 Site Climatology

- 5 The reference meteorological mast MP5 has eight years of continuous wind speed and wind direction measurements from a calibrated cup anemometer and wind vane at 118 m agl. Figure 5a shows the wind climatology with a wind rose from the period between February 2011 to January 2019. The Alaiz mountain top presents a mean wind speed of 8.6 m s^{-1} at 118 m with a turbulence intensity of 7% at 15 m s^{-1} as well as a bidirectional regime, with prevailing winds from a north-northwest sector ($330^\circ\text{--}360^\circ$, 32% of total) and a south-southeast sector ($150^\circ\text{--}180^\circ$, 23% of total).
- 10 Figure 5b shows the wind rose of ALEX17 two years' extensive measurement period, from July 2017 to July 2019, which has a representative wind regime when compared with the long-term climatology. As the MP5 is located next to the wind turbines during power curve measurements, it is susceptible to wind turbine wake effects with winds between 130° to 240° (see figure 3).

In complex terrain, the characterization of spatial variability is critical to capture a full picture of the wind regime. Figure 15 6a illustrates this with the wind rose measured at the valley floor by M5 during the EMP. Comparing the mountain top (Fig. 5) with the valley floor (Fig. 6a), we observe a turning effect with NW and SE valley winds. Higher wind speeds come from SE confirming the funnel effect caused by the valley conical section with a larger area facing west (see figure 2b). Furthermore,

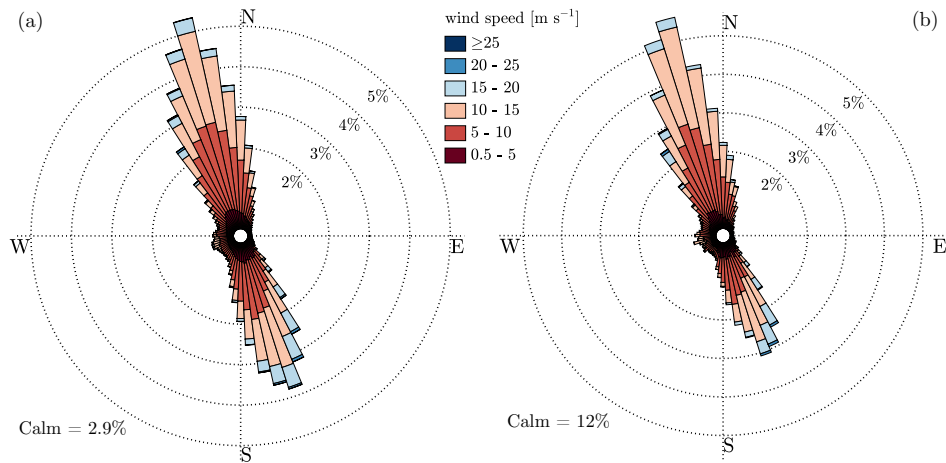


Figure 5. Wind roses of 10-min wind speeds observed by MP5 at 118 m for the reference period (2011-2019) (a) and during the EMP (b). The calm threshold is 0.5 m s^{-1} . Each bin contains a 5° wind direction interval and circular grid labels indicate the percentage of occurrence.

the turbulence intensity is higher at the valley floor when compared to the mountain top, being 11% at 15 m s^{-1} at 80 m from M5 observations.

The combination of topographic features $\mathcal{O}(10 \text{ km})$ away and elevation changes up to 700 m between the valley floor and mountain top poses a challenge to numerical models such as the Weather Research and Forecast (WRF) model. The NEWA project delivered a wind atlas for all European countries using WRF with a horizontal and temporal resolution of 3 km and 30 min, respectively (Hahmann et al., 2020; Dörenkämper et al., 2020). Here called NEWA-WRF, this model output is publicly available and covers a 30-yr period (1989–2018).

Figure 6b compares the wind distribution measured at MP5 during both the long-term reference period (February 2011–January 2019) and the EMP (July 2017–July 2019) with the simulated distribution from NEWA-WRF also from the long-term period. The model output was extracted at the MP5 position using a linear interpolation of the nearest neighbor grid cells as well as the nearest vertical levels. Results show that the NEWA-WRF simulations underestimate the mean wind by more than 1.5 m s^{-1} which is indicative of unresolved speed-up effects in the meso-scale model. The measured wind distribution further confirms that the EMP ~~can represent the wind climate~~ contains a representative set of meteorological conditions.

An extensive study evaluated the mean wind speed bias between measurements and NEWA-WRF simulations using 291 onshore masts over Europe, where complex sites are defined as having 2% of their slopes higher than 16.7° within a radius of 3.5 km (Dörenkämper et al., 2020). Results showed that the selected NEWA-WRF setup in complex sites has a mean wind speed bias of $-0.25 \pm 0.83 \text{ m s}^{-1}$. Based on Fig. 6b, ALEX17 has a much larger systematic underestimation of the wind speed when compared to NEWA-WRF’s validation study, as expected since ~~the complexity~~ at MP5 is ten-times higher based on the same criteria 20% of the slopes exceed 16.7° . In order to improve modeling here we need to further downscale NEWA-WRF using non-linear micro-scale models.

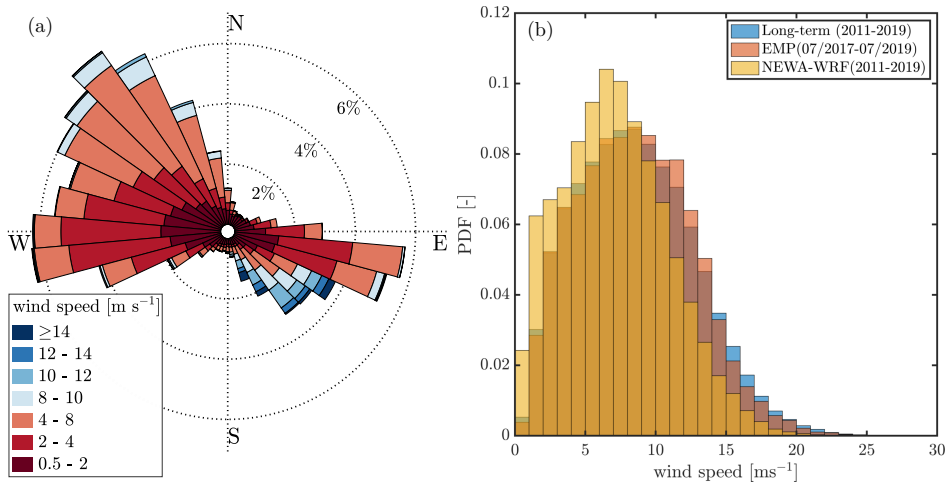


Figure 6. Panel (a) shows the wind rose of 10-min wind speeds at the valley measured by M5 at 80 m agl. Panel (b) shows the wind speed distributions at 118 m agl measured at MP5 during the reference period and EMP along with the modeled wind speeds from NEWA-WRF for the reference period.

3.2 Atmospheric stability

Monin-Obukhov Similarity Theory (MOST) is commonly used to describe the mean and turbulence characteristics of the flow within the surface layer (Foken, 2006). MOST assumes that over horizontally homogeneous and flat terrain (HHF) conditions, normalized atmospheric gradients such as those of wind and temperature are functions of the dimensionless parameter z/L , where z is the height above ground and L is the Obukhov length, which is defined [here](#) as $L = -(u_*^3 T_s) / (\kappa g \overline{w' T_s'})$, where $u_* = (\overline{u' w'^2} + \overline{v' w'^2})^{1/4}$ is the friction velocity, $\kappa = 0.4$ the von Kármán constant, g the acceleration due to gravity and T_s the sonic anemometer temperature. The prime ($'$) denotes fluctuations and the overbar a mean. The velocity components u , v and w refer to the stream-wise, cross-wind and vertical velocity components, respectively.

In ALEX17 we select the central position as a reference for atmospheric stability and we use z/L to evaluate the wind profiles under different stability conditions for two predominant wind directions. The CP is located on a plateau within the valley floor surrounded by farmland, which is one of the flattest and most homogeneous areas in the experimental area, but still far from HHF conditions. The climatology of stability is derived by computing z/L at 10 m agl from sonic anemometer measurements at 20 Hz, computing the fluxes over 30 minutes. We use the coordinate system described above by applying yaw and pitch rotations, i.e. double rotation. Table 2 shows the atmospheric stability classes given by z/L intervals following the analysis by Berg et al. (2011) and the number of 30-min profiles. [The \$z/L\$ parameter was chosen to classify stability from a climatological point of view. For the stratified flow patterns over complex terrain \(section 4\), we select the Froude number since it is a more descriptive parameter for flow over obstacles \(Kaimal and Finnigan, 1994\).](#)

The M7's 3D sonic anemometer closest to the surface is at 10 m agl. One-year of measurements (from August 2018 to July 2019) are available from this sonic anemometer with 84.6% of valid 30-min periods. Figure 7a shows the daily cycle

Stability class	z/L	# of 30-min profiles
unstable (u)	$z/L \leq -0.2$	572
near unstable (nu)	$-0.2 < z/L < -0.04$	904
neutral (n)	$ z/L \leq 0.04$	1447
near stable (ns)	$0.04 < z/L < 0.2$	1115
stable (s)	$z/L \geq 0.2$	1054

Table 2. Definition of atmospheric stability classes within intervals of z/L and respective quantity of 30-min profiles.

of dimensionless stability $10/L$ at M7. As expected, stably stratified conditions prevail at night, whereas unstable conditions dominate during daytime and peak around midday. Figure 7b shows the behavior of stability with wind speed, where a prevalence of neutral conditions with increasing wind speeds is found. [We have also performed a similar analysis using the gradient Richardson number with concurrent wind speed observations from M7 and potential temperature profiles from the WindRASS.](#)

5 [This parameter showed a similar distribution of stability classes in terms of diurnal cycle and wind speed bins \(not shown\).](#)

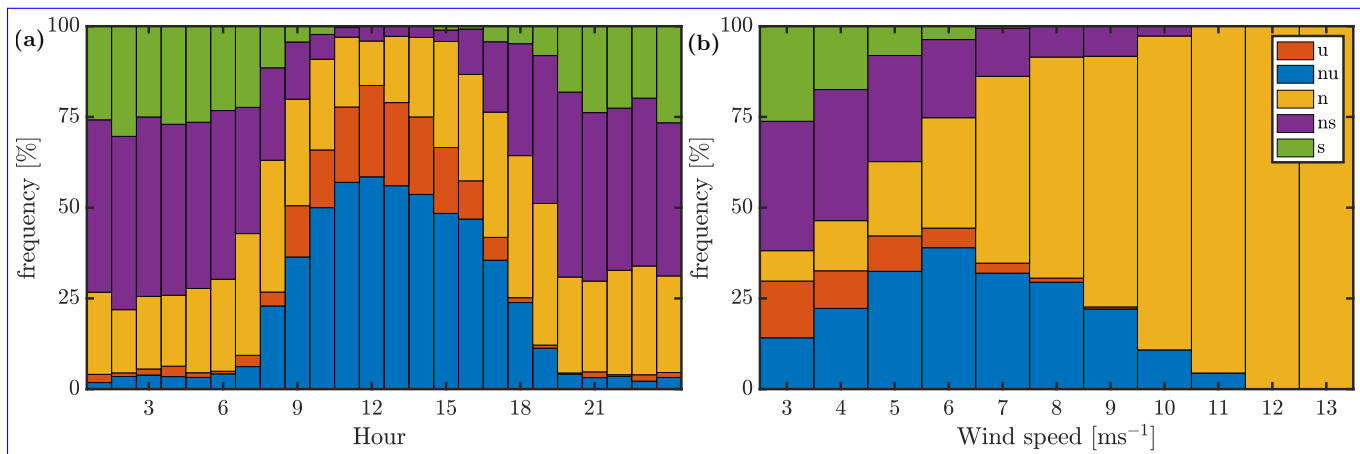


Figure 7. Frequency of z/L at 10 m agl divided in stability classes per hour (a) and per wind speed (b) from measurements at M7. The stability classes are found in table 2. [The time is in UTC.](#)

Figure 8 presents the vertical profiles of the normalized mean wind speed for two prevalent wind sectors at the valley floor, namely a NW sector ($300^\circ \pm 30^\circ$) [with 3193 30-min profiles in total](#) and a SE sector ($120^\circ \pm 30^\circ$) [with 3120 30-min profiles](#), both divided by stability classes. [For the each vertical level, the shaded area represents the standard error of the mean given by \$\pm\sigma/\sqrt{N}\$, where \$\sigma\$ is the standard deviation and \$N\$ the number of observations.](#) For the SE sector (Fig. 8a) large differences can be observed close to the surface, showing that the surface roughness' fetch can be quite inhomogeneous for this sector but also likely influenced by [land-cover](#) seasonal effects. Also, negative wind shears characterize the stable class, which are potentially caused by valley drainage flow (Serafin et al., 2018). Profiles from the NW wind sector (Fig. 8b) resemble more

flat and homogeneous conditions, with increasing wind shear with stability and a similar normalized wind close to the surface except for stable conditions.

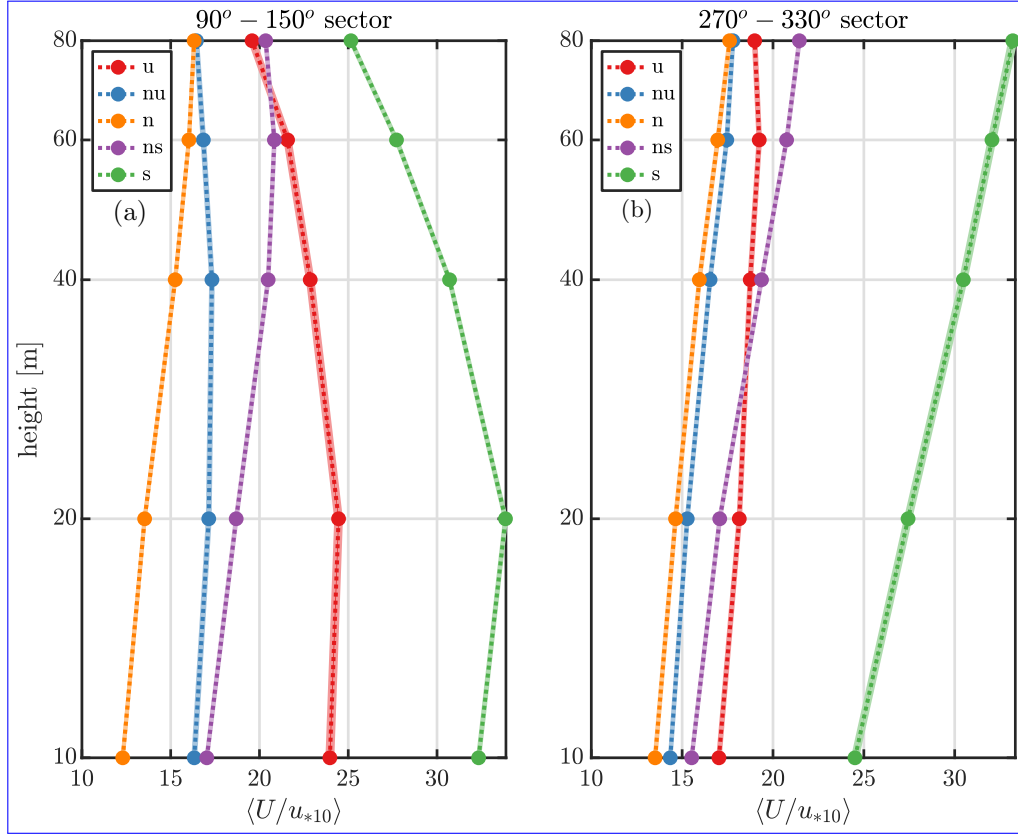


Figure 8. Mean vertical wind profiles normalized with the friction velocity computed by the 10-min sonic anemometer (u_{*10}). Panel (a) shows profiles within the $120^\circ \pm 30^\circ$ sector and panel (b) shows profiles within the $300^\circ \pm 30^\circ$ sector based on wind directions at 10m. Shaded areas denote associated standard errors of the mean.

Furthermore, when dealing with mountain flows, the topography occupies a large portion of the ABL and hence plays a major role in the flow stratification. Disturbances in the stable atmosphere caused by the topography may generate three-dimensional flow phenomena i.a. atmospheric lee waves, rotors and hydraulic jumps (Kaimal and Finnigan, 1994). The natural frequency of these vertical oscillations is characterized by the Brunt-Väisälä frequency $N = [(g/\bar{\theta})(\partial\bar{\theta}/\partial z)]^{1/2}$ where $\partial\bar{\theta}/\partial z$ is the potential temperature gradient. The potential temperature is computed as $\theta = T + 0.0098z_{asl}$, where 0.0098 Km^{-1} is the dry adiabatic temperature gradient. The potential temperature gradient in N is calculated by linear interpolation between the measurements at 2 and 80 m for M5/M3 and between 2 and 113 m for MP5.

10 The Froude number (Fr) is the dimensionless parameter given by the ratio of flow inertia based on a reference upwind wind speed U to the gravity forces acting on the flow (Kaimal and Finnigan, 1994). Following the linearized solution presented by

Rotunno and Lehner (2016) $Fr = \pi U / 2ND$, where D is a height for the stably stratified flow layer upstream of the mountain, also called inversion depth. The $\pi/2$ multiplier comes from a derivation considering critical flow, i.e., $Fr = 1$. The scaling can also be performed with a characteristic mountain height H .

We ~~select the characteristic height H as the elevation difference between MP5 and M7, which is ≈ 500 m. The~~ choose the inversion depth D ~~is assumed~~ to be proportional to the high wind speed layer height from the lidar measurements (c.f. figure 9) ~~and equal to 500 m, i.e., it is an empirical selection based on this case study. The characteristic height H is considered as the elevation difference between MP5 and M7, which is ≈ 500 m,~~ hence $H \sim D \approx 500$ m. Fr is evaluated at the Alaiz mountain top (MP5) and foothills (M2), at the valley floor (M5) and at the north ridge slope (M3) using the same D . ~~The potential temperature gradient in N is calculated by linear interpolation between the measurements at 2 and~~ Furthermore, the characteristic wind speed U is taken at 80 m for M5/M3 and between 2 and 113 m for MP5. Hereat all positions.

It is worth noticing that the computation of Fr in this study has some caveats, as neither U nor N represent the entire inversion depth and D is a characteristic length with a somewhat arbitrary value. Here, our aim is to investigate the relative changes in Fr , where we compare Fr estimations at the mountain top ~~and with the ones~~ along the valley.

4 Selected flow cases

4.1 The Lee-Side Hydraulic Jump

An atmospheric hydraulic jump occurs when a two-layer stratified flow encounters an obstacle and experiences ~~a discontinuity an abrupt and turbulent transition~~ in the flow layer depth and velocity, causing dissipation of kinetic energy in order to recover part of the original potential energy that existed upstream ~~It (Kaimal and Finnigan, 1994). It is assumed that the hydraulic theory can describe these high-amplitude mountain waves with downslope flow in the lee side (Baines, 1995).~~ It differs from atmospheric gravity waves or lee waves since it involves a ~~stronger~~ discontinuity and requires non-linear dynamics to be described, analogous to a shock wave when sound crosses the Mach number. ~~Hence, it is assumed that the hydraulic theory can describe these high-amplitude mountain waves with downslope flow in the lee side (Baines, 1995).~~

Long (1954) performed water tunnel experiments and his results show that the lee-side hydraulic jump occurs when the topographical feature is comparable to the depth of the upstream flow layer and there is a Fr transition between supercritical (> 1) at the mountain top and subcritical (< 1) in the lee-side. The solutions presented by Houghton and Kasahara (1968) and Vosper (2004) also predicted under which conditions the jump occurs, based on H , D and a Fr scaled with the maximum wave speed given by $\sqrt{gD}\sqrt{g'D}$, where g' is a reduced gravitational acceleration.

METCRAX II identified jump-like episodes using co-planar RHI lidars scans (Lehner et al., 2016). Whiteman et al. (2018) used the latter lidar measurements to propose a conceptual model of the jump, yet limited to the scales and particularities of the meteorite crater case study. Rotunno and Bryan (2018) further performed numerical simulations of a steady-state jump considering the full time-dependent three-dimensional flow description. Results quantify the jump's evolution and structure based on potential temperature, vorticity and turbulent kinetic energy.

We defined $H \sim D \approx 500$ m in section 3.2, which ~~agrees with previous studies (Sanz-Rodrigo et al., 2013).~~ is arbitrary using observations from this episode. Therefore, this choice can produce variations in the Froude number. Figure 9 shows four 10-min periods of co-planar RHIs during one night where a hydraulic jump was spotted at the lee side of the Alaiz mountain between October 5th and 6th 2018.

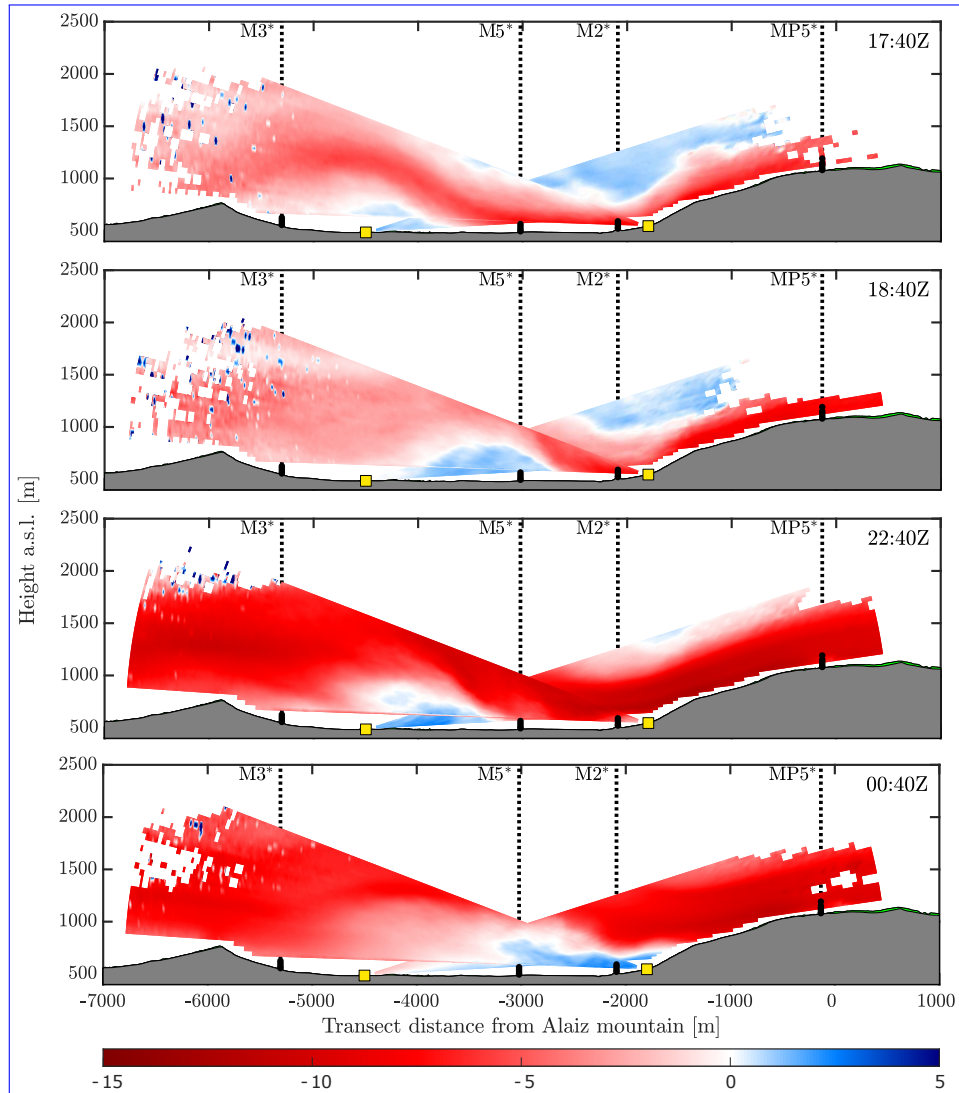


Figure 9. Superposition of dual RHI scans during the hydraulic jump period between 5th–6th October 2018. The color bar represents radial wind speed in ms^{-1} with negative values representing flow from right to left. Each of the frames correspond to a 10-min scan.

- 5 The main southerly flow has negative radial wind speeds, indicated by red colors, where a strong downslope wind reaches the valley and performs the jump, which is non-steady as the jump location changes with time. Long (1954) also argued that

when Fr decreases at the obstacle, the jump moves towards the obstacle (mountain) and loses intensity. Conversely, when Fr increases at the obstacle, the jump moves further downstream and becomes more intense.

Figure 10 compares the wind direction regimes and Fr numbers between the masts located at the mountain top (MP5), mountain foothills (M2), valley floor (M5) and north ridge's slope (M3). The M7 mast did not have valid temperature measurements during this period, hence it is not shown. The southerly flow is maintained at MP5 throughout the period, with easterly winds at the jump's location. We observe a transition between $Fr > 1$ at the mountain top to $Fr < 1$ at the valley. According to Long (1954), the supercritical to subcritical transition is strong evidence for the onset of a hydraulic jump, which is confirmed herein as well as in smaller scale experiments (Rotunno and Lehner, 2016).

Furthermore, the time evolution of the hydraulic jump described by Long (1954) is also confirmed in this episode. Between 18:40Z and 22:40Z the jump tends to move further downstream as Fr at MP5 goes from 1 to 1.5. From 22:40Z to 00:40Z the flow loses intensity, the jump moves towards the mountain while Fr at MP5 decreases from 1.5 to 1.2, and the M2 measurements evidence a recirculation zone in the lee-side of the mountain, in the lower portion of the hydraulic-jump rotor, evidence reverse surface winds (Strauss et al., 2016). Nonetheless, towards the end of this episode the lidar measurements cease to show strong downslope winds into the valley. The last scan of figure 9 suggests that the flow tends to evolve to a lee-wave-type rotor, with Fr closer to critical at the mountain top (c.f. Fig. 10b) and less of a closed rotor circulation downstream.

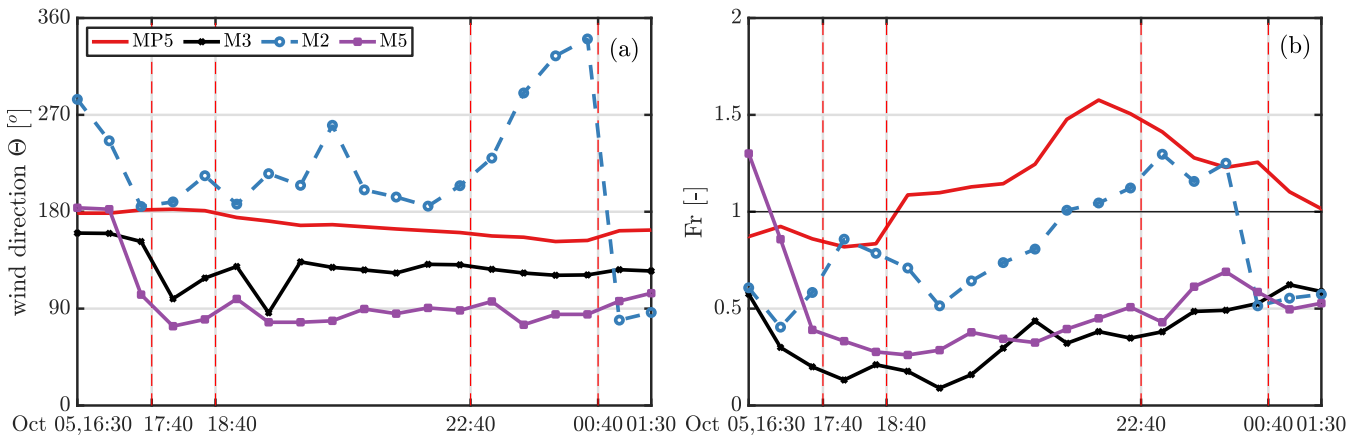


Figure 10. Time series of wind direction (a) and Froude number (b) during the hydraulic jump case. The vertical dashed lines represent the snapshots of figure 9.

Figure 11a shows a 10-min average snapshot (19:00Z) of the hydraulic jump episode, with wind and temperature measurements from the surface-layer stations. The stratified southerly winds close to the surface enter the Elorz valley surrounding the Alaiz mountain through the eastern side. The flow at the center of the valley (from S3, S8, S1 and S2) is from the east. The wind speed from the along-valley stations also shows the effect of topographical channeling, i.e. the wind decelerates as the valley becomes wider. On the other hand, the flow along the Alaiz slopes comes from the south (see S5, S4 and S6) and remains

almost steady along the night. Wind at the northern part of the valley is weak, which is also observed by the lidar scans, and the air stratification is more intense, as shown by S7 and S9, located downstream the hydraulic jump.

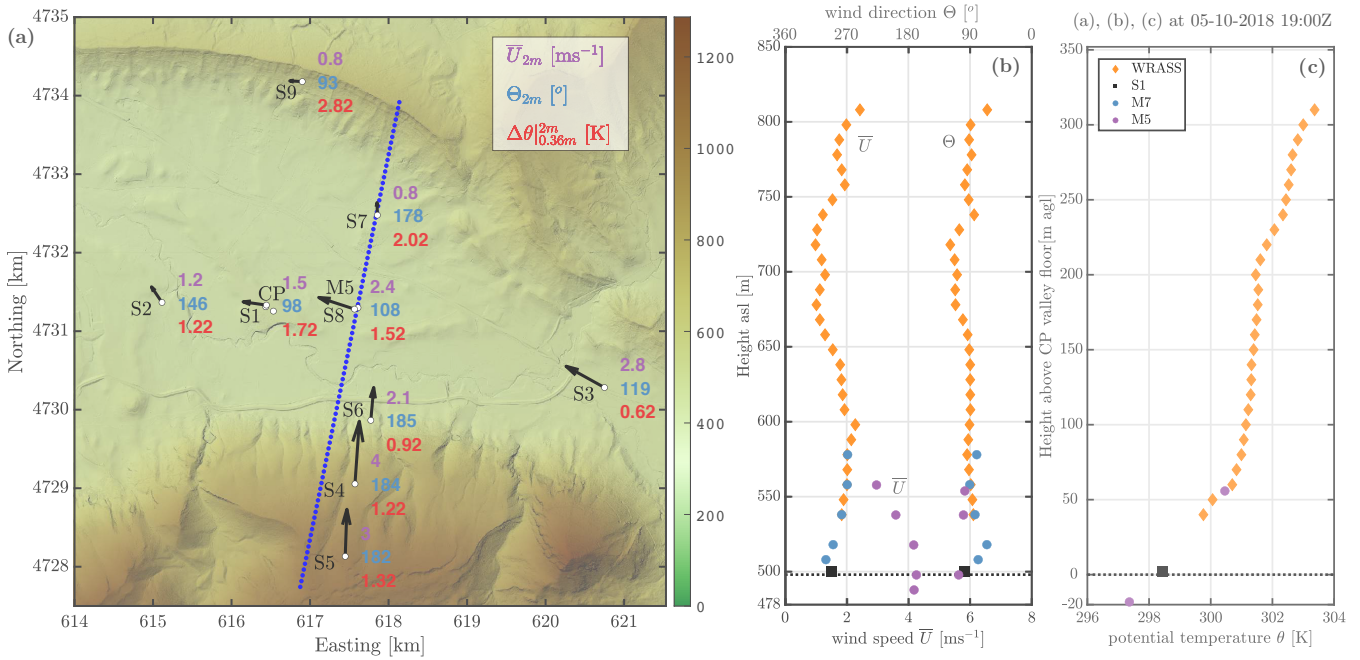


Figure 11. Wind conditions during hydraulic jump case at 05-10-2018 19:00Z. Panel (a) shows surface-layer-surface layer stations' wind speed (\bar{U}_{2m}), wind direction (Θ_{2m}), both at 2 m and potential temperature measurementsgradient between 0.36 m and 2 m ($\Delta\theta$). Panels (b) and (c) show vertical profiles of wind and potential temperature at the valley from the sodar RASS, M7, S1 and M5. The dashed line marks the valley floor level at CP.

Figure 11b shows the same 10-min snapshot (19:00Z) of wind speed and direction profiles from S1, M7, M5 and sodar RASS at the central position. The instruments at the CP agree and show quiescent-weak easterly winds. Additionally, the wind speed profile at M5 further highlights the valley channeling effect, with measurements located 1 km east and 20 m below CP. The potential temperature profiles (figure 11c) from S1, M5 and sodar RASS agree and show a stable-boundary-layerthermal inversion. The presence of a stratified valley floor with stagnant flow agrees with similar observations of METCRAX II (Lehner et al., 2016), but here in a horizontal scale ten times larger.

This case shows that the lee-side hydraulic jump is characterised by a Fr transition from supercritical $Fr > 1$ at the mountain to subcritical $Fr < 1$ at the valley floor. After inspecting the entire year period with concurrent data from MP5 (mountain top) and M5 (valley floor), approximately 35% of all the stably stratified periods reproduce a similar Fr transition. Thus, considering only southerly winds, the occurrence of the hydraulic jump could reach 10% of the time, suggesting that the current dataset could be suitable for a deeper study on such phenomena.

4.2 Layered flow induced by valley winds

During the hydraulic jump we have seen how winds at the valley characterized the jump's recirculation zone. Disparately, with low wind speeds thermal stratification over mountainous terrain can modulate flow patterns (Jiménez et al., 2019) ~~due to the~~ which, together with a heterogeneous land cover, ~~which~~ causes unequal heat fluxes (Martínez et al., 2010). Grubišić et al. (2008) showed a three-layer flow structure in a valley-mountain region under quiescent conditions, where up-valley and down-valley winds are thermally driven and decoupled from the meso-scale flow aloft. ALEX17 also presents valley winds that develop into layered stratified flows.

An example is found during the night of October 24th to 25th 2018. For this case, the synoptic situation is dominated by a strong wind of northern component whose intensity starts to decrease several hours after sunset. Closer to the surface, this general wind takes a western direction within the Elorz valley. Figure 12a shows four 10-min periods of the co-planar RHI scans representative of the evolution of the layered flows within the valley. As in figure 9, the positive radial wind speeds represent flow from left to right. Figure 12b displays the corresponding potential temperature profiles measured by the sodar RASS and M5 at the valley center, where the air becomes cooler close to the surface and a thermal inversion develops along the night, becoming very intense after midnight.

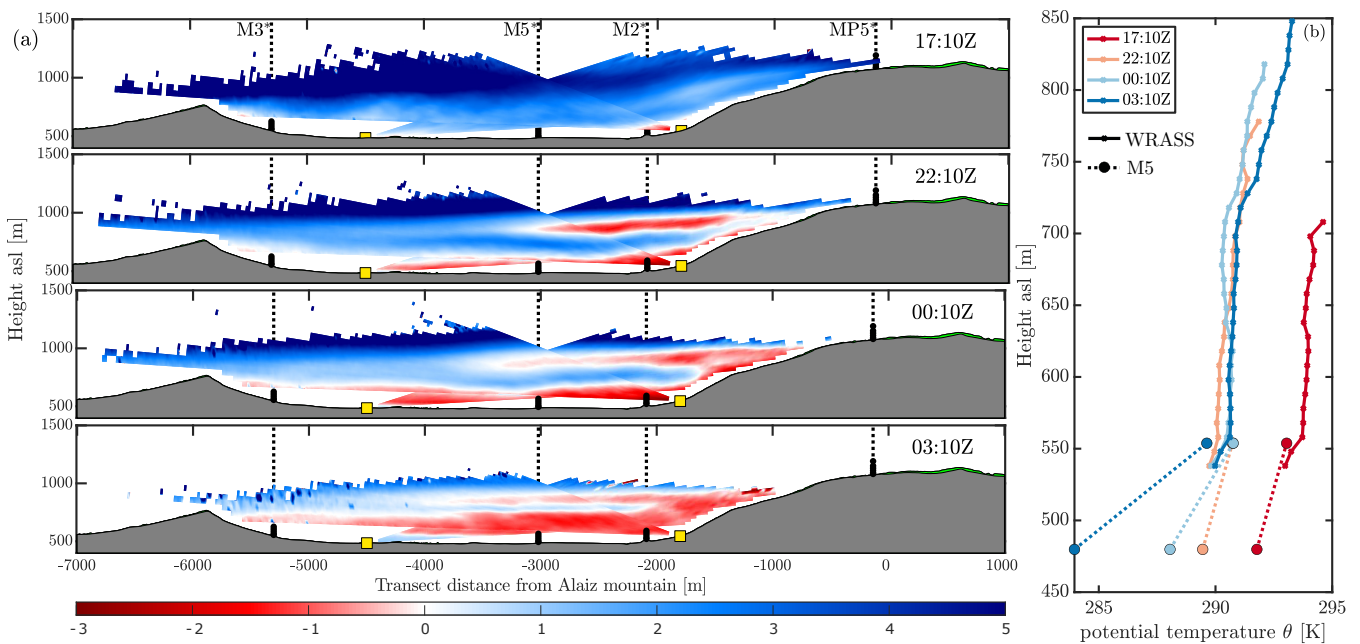


Figure 12. Panel (a) shows the superposition of dual RHI scans during the layered valley winds period between 24th–25th October 2018. Panel (b) shows the potential temperature profiles measured by the sodar RASS and M5 at each frame in (a).

15 Before sunset ($\approx 17Z$), the northwesterly flow within the valley is coupled with stronger mountain winds aloft as shown by the first lidar scan. A weak stably stratified layer develops after sunset and surface winds adjust to a new equilibrium where

the valley topography has a major influence. This layer depth increases as the thermal inversion develops within the valley, producing a layering effect as seen by the subsequent RHI scans [at 22:10Z and 00:10Z](#) (figure 12a). Southwesterly winds are present at the valley floor and over the southern slopes, while a northwesterly flow remains within the valley atmosphere aloft, still coupled with the mesoscale wind. Both layers are stably stratified although with different intensity. The thermal stratification at the upper layer remains steady along the night, while the surface inversion evolves very slowly until midnight (figure 12b).

Figure 13a shows a 10-min average snapshot (22:30Z) of the valley winds measured by the surface-layer stations, indicating the southerly component of the wind at the valley center and over the southern slope within the surface layer, as well as the increment of the wind speed as the valley gets narrower towards the east. The S7 and S9 positions show a [recirculation-sheltered](#) zone in the lee-side of the north ridge, where the wind is very weak together with the strongest surface thermal inversion.

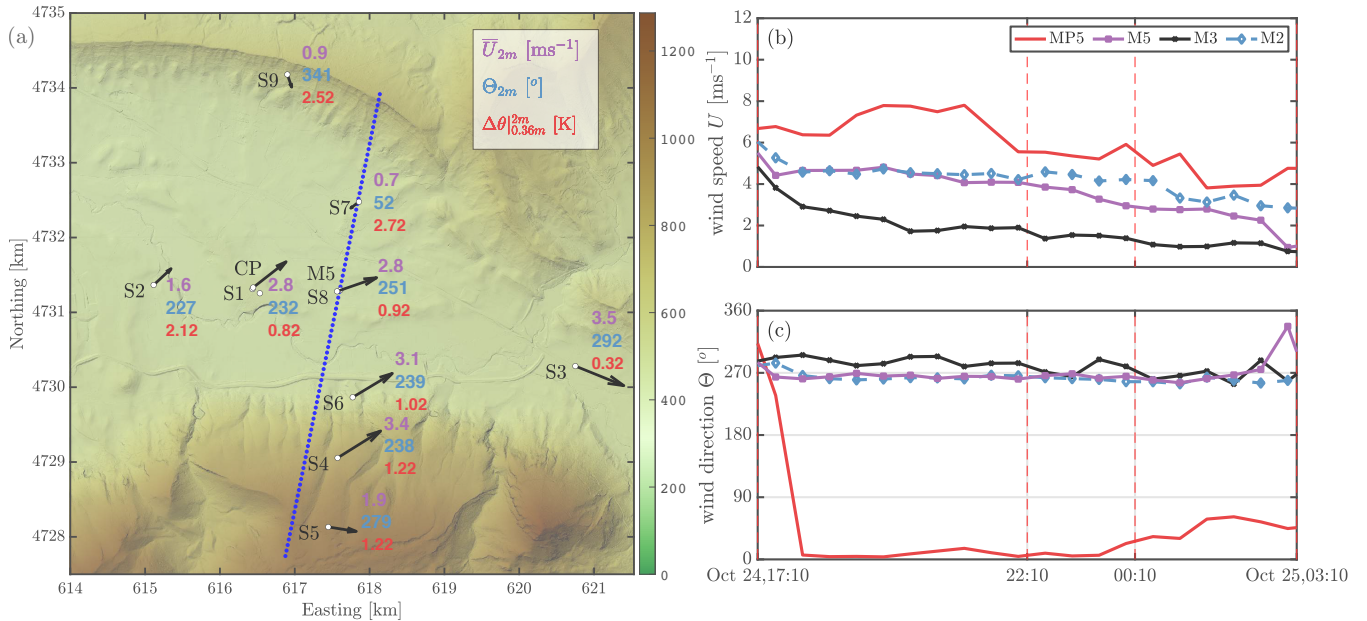


Figure 13. Panel (a) shows surface layer stations' wind speed (\bar{U}_{2m}), wind direction (Θ_{2m}), both at 2 m and potential temperature measurements-gradient between 0.36 m and 2 m ($\Delta\theta$) at 24-10-2018 22:30Z. Panels (b) and (c) show the time series of wind speed and direction from the masts, respectively. The vertical dashed lines represent the snapshots of figure 12.

Figures 13b and c represent the wind speed and wind direction measured at MP5 118 m agl and at 80 m agl by distinct masts across the valley. There is a persistent offset of 90° in the wind direction between the mountain (MP5) and valley (M2,M3,M5), while the general wind decreases throughout the evening, as indicated by MP5. In consequence, the wind speed also diminishes within the valley, intensifying the surface cooling and generating a stronger thermal inversion at the valley floor after midnight (figure 12b). This situation [favours the development of a cold air pool](#) (Serafin et al., 2018) which decouples the surface layer, with winds responding to a local regime, from the southwesterly flow within the valley (not shown). An elevated thermal

inversion around 720 m asl ~~decouples the valley atmosphere from the northerly wind aloft~~ (see profile at 03:10Z in figure 12b) decouples the valley atmosphere from the northerly wind aloft, increasing the depth of the red band within the valley observed in the RHI scan at 03:10Z (figure 12a).

5 Summary and Conclusions

5 This work ~~presents~~ introduces the Alaiz Experiment (ALEX17) with details on the main innovations in atmospheric measurements, unique characteristics and two flow patterns observed during the eight-month Intensive Observational Period (IOP). ALEX17 is in a striking position in terms of scale and complexity. The experimental domain is large enough for synoptic effects to be essential for flow modeling while still being within the range of current long-range commercial lidars.

10 Additionally, ALEX17 requires the adoption of meso- to micro-scale models. Palma et al. (2019) showed advancements in such modeling schemes during the Perdigão experiment, especially for stably stratified flows. ALEX17 yet poses a further challenge in numerical modeling efforts ~~for~~ because of its large domain size.

The topographical features of ALEX17, with a non-parallel mountain-valley-ridge configuration, lead to the occurrence of valley winds with quite distinct wind regimes from the mountain top, where wind ~~direction offsets~~ rotates by up to 90° and channeling effects being observed. To capture most of the wind flow spatial variability, five WindScanners performed synchro-
15 nized measurements of a unique 10-km transect line, covering a vast portion of the experimental domain. The experimental report (Cantero et al., 2019) offers further technical information on the campaign and dataset (Cantero et al., 2019).

Wind measurements at the mountain top are available since 2011, nevertheless ALEX17's two years extensive measurement campaign has been able to represent well the wind climatology. When comparing available meso-scale modeling from the New European Wind Atlas with observations, a negative bias in the mean wind larger than 1.5 m s^{-1} pointed to the need of further
20 improvement of model performance at this site. At the valley floor, vertical wind profiles with southeasterly winds showed negative wind shear under stable conditions, whereas for northwesterly wind profiles are more canonical but still affected by land cover inhomogeneities.

Using the multi-lidar scans we spotted a lee-side atmospheric hydraulic jump episode. Measurements from masts and surface-layer stations corroborated the formation and evolution of the jump with long-established predictions (Long, 1954).
25 The Froude number transition from supercritical (> 1) to subcritical (< 1) was quantified and results suggest that this type of stratified atmospheric wave can potentially happen during $\approx 10\%$ of the time in this site.

The hydraulic jump is connected with high southerly winds at the mountain top. On the other hand, during stratified conditions with lower wind speeds, valley winds become decoupled from the mountain flow aloft due to thermal stratification, favouring the formation of a cold air pool very close to the surface (Martínez et al., 2010; Conangla et al., 2018). This case is
30 illustrated with a layered flow pattern measured by the lidar scans, where westerly stratified valley winds interact with northerly winds aloft. Other atmospheric phenomena captured within the IOP shall be the object of further studies.

We have characterized two multi-scale stratified flows regarded as challenging both in terms of ~~its~~ their physical description (Serafin et al., 2018) and modeling (Sanz Rodrigo et al., 2017). Other flow episodes, featuring i.a. upstream flow blockage and

lee waves, were spotted and can be the object of further studies. These measurements will provide aid to evaluate numerical models especially for testing the effects of atmospheric stability on flow over complex terrain.

Data availability. The Alaiz Experiment dataset collected during the EMP is publicly available and can be found in Santos et al. (2019), with metadata and citation guidelines for each group of instruments.

- 5 *Author contributions.* Funding acquisition and project administration: J.M., J.S.R., J.C., E.C. Conceptualization and resources: J.M., J.S.R., E.C., P.S., N.V., J.C. and D.M-V. Data curation: P.S., D.M-V., F.B.G. and E.C. Methodology: P.S., N.V. and D.M-V. Formal analysis and visualization: P.S. and B.M. Writing - original draft: P.S. Writing - review & editing: P.S., J.M., N.V., E.C., J.S.R., F.B.G., D.M-V., B.M. and J.C.

Competing interests. The authors declare no conflict of interest.

- 10 *Acknowledgements.* We would like to thank Michael Courtney and all staff from DTU Wind Energy (Denmark), CENER and UIB (Spain) involved on the commissioning and ongoing monitoring of the experimental infrastructure. We credit Alfredo Peña for reviewing the manuscript and for the analysis that resulted in Figure 1. We would also like to thank Ebba Dellwik for her guidance during the manuscript writing, Bianca Adler for her useful comment during the open discussion and two anonymous referees for a thorough review. The European Commission (EC) partly funded NEWA project (NEWA- New European Wind Atlas, FP7-ENERGY.2013.10.1.2, European Commission's
15 grant agreement number 618122). National agencies that also provided funding are the Danish Energy Agency and Ministerio de Economía y Competitividad (Spain). B.M. was supported by the grant FPI-CAIB (FPI/2165/2018) of the Vicepresidència i Conselleria d'Innovació, Recerca i Turisme del Govern de les Illes Balears and the Fons Social Europeu. The WindRASS and SEB station were rented from the Meteorological Service of Catalonia with funds of the research project PCIN-2014-016-C07-01.

Appendix A: Lidar configuration for RHI transect scan

- 20 ~~We would like to thank Michael Courtney and all staff from DTU Wind Energy (Denmark), CENER and UIB (Spain) involved on the commissioning and ongoing monitoring of the experimental infrastructure. We credit Alfredo Peña for the analysis that resulted in Figure 1. The European Commission (EC) partly funded NEWA project (NEWA- New European Wind Atlas, FP7-ENERGY.2013.10.1.2, European Commission's grant agreement number 618122). National agencies that also provided funding are the Danish Energy Agency and Ministerio de Economía y Competitividad (Spain). B.M. was supported by the grant~~
25 ~~of the Vicepresidència i Conselleria d'Innovació, Recerca i Turisme del Govern de les Illes Balears.~~

Parameters	WS3	WS5
(Easting, Northing) [m]	(617846.80,4732496.43) m	(617305.59,4729848.75) m
Elevation [m asl]	487.21 m	545.92 m
Azimuth [$^{\circ}$]	191.55 $^{\circ}$	11.55 $^{\circ}$
Elevation (min,max) $^{\circ}$	(3 $^{\circ}$,18 $^{\circ}$)	(1.58 $^{\circ}$,21.56 $^{\circ}$)
Scan speed [$^{\circ}s^{-1}$]	0.5 s^{-1}	0.666 s^{-1}
Range gates [min: Δ :max] m	[100:50:5000] m	[100:20:5000] m
Accumulation time [ms]		1000 ms
Pulse length [ns]		400 ns
Points per range gate [-]		128
Signal spectral width [ms^{-1}]		3 ms^{-1}
Specified physical resolution [m]		75 m

Table A1. Windscanner’s position and configuration for the Transect RHI scans.

References

- Adler, B., Gohm, A., Kalthoff, N., Babić, N., Corsmeier, U., Lehner, M., Rotach, M. W., Haid, M., Markmann, P., Gast, E., Tsaknakis, G., and Georgoussis, G.: CROSSINN - a field experiment to study the three-dimensional flow structure in the Inn Valley, Austria, *Bulletin of the American Meteorological Society*, pp. 1–55, <https://doi.org/10.1175/BAMS-D-19-0283.1>, 2020.
- 5 Badger, J., Frank, H., Hahmann, A. N., and Giebel, G.: Wind-climate estimation based on mesoscale and microscale modeling: Statistical-dynamical downscaling for wind energy applications, *Journal of Applied Meteorology and Climatology*, 53, 1901–1919, <https://doi.org/10.1175/JAMC-D-13-0147.1>, 2014.
- Baines, P. G.: *Topographic Effects in Stratified Flows*, Cambridge University Press, Cambridge, 1995.
- Bechmann, A., Sørensen, N. N., Berg, J., Mann, J., and Réthoré, P. E.: The Bolund Experiment, Part II: Blind Comparison of Microscale
- 10 Flow Models, *Boundary-Layer Meteorology*, 141, 245–271, <https://doi.org/10.1007/s10546-011-9637-x>, 2011.
- Berg, J., Mann, J., Bechmann, A., Courtney, M. S., and Jørgensen, H. E.: The Bolund Experiment, Part I: Flow Over a Steep, Three-Dimensional Hill, *Boundary-Layer Meteorology*, 141, 219–243, <https://doi.org/10.1007/s10546-011-9636-y>, 2011.
- Cantero, E., Borbón Guillén, F., Sanz Rodrigo, J., Santos, P., Mann, J., Vasiljević, N., Courtney, M., Martínez Villagrasa, D., Martí, B., and Cuxart, J.: Alaiz Experiment (ALEX17): Campaign and Data Report, Tech. Rep. May, <https://doi.org/10.5281/zenodo.3187482>, 2019.
- 15 Chavez Arroyo, R. A.: ALEX17 high-resolution, digital information of topography, surface and aerodynamic roughness of the experimental domain, <https://doi.org/10.11583/DTU.8143775.v1>, 2019.
- Conan, B., Chaudhari, A., Aubrun, S., van Beeck, J., Hämäläinen, J., and Hellsten, A.: Experimental and Numerical Modelling of Flow over Complex Terrain: The Bolund Hill, *Boundary-Layer Meteorology*, 158, 183–208, <https://doi.org/10.1007/s10546-015-0082-0>, 2016.
- Conangla, L., Cuxart, J., Jiménez, M. A., Martínez-Villagrasa, D., Miró, J. R., Tabarelli, D., and Zardi, D.: Cold-air pool evolution in a wide
- 20 Pyrenean valley, *International Journal of Climatology*, 38, 2852–2865, <https://doi.org/10.1002/joc.5467>, 2018.
- Coppin, P. A., Bradley, E. F., and Finnigan, J. J.: Measurements of flow over an elongated ridge and its thermal stability dependence: The mean field, *Boundary-Layer Meteorology*, 69, 173–199, <https://doi.org/10.1007/BF00713302>, 1994.

- Cuxart, J., Cunillera, J., Jiménez, M. A., Martínez, D., Molinos, F., and Palau, J. L.: Study of Mesobeta Basin Flows by Remote Sensing, *Boundary-Layer Meteorology*, 143, 143–158, <https://doi.org/10.1007/s10546-011-9655-8>, 2012.
- Cuxart, J., Conangla, L., and Jiménez, M. A.: Evaluation of the surface energy budget equation with experimental data and the ECMWF model in the Ebro Valley, *Journal of Geophysical Research*, 120, 1008–1022, <https://doi.org/10.1002/2014JD022296>, 2015.
- 5 Dörenkämper, M., Olsen, B. T., Witha, B., Hahmann, A. N., Davis, N. N., Barcons, J., Ezber, Y., García-Bustamante, E., González-Rouco, J. F., Navarro, J., Sastre-Marugán, M., Sile, T., Trei, W., Žagar, M., Badger, J., Gottschall, J., Sanz Rodrigo, J., and Mann, J.: The Making of the New European Wind Atlas – Part 2: Production and evaluation, *Geoscientific Model Development*, 13, 5079–5102, <https://doi.org/10.5194/gmd-13-5079-2020>, 2020.
- Fernando, H. J., Pardyjak, E. R., Di Sabatino, S., Chow, F. K., De Wekker, S. F., Hoch, S. W., Hacker, J., Pace, J. C., Pratt, T., Pu, Z.,
10 Steenburgh, W. J., Whiteman, C. D., Wang, Y., Zajic, D., Balsley, B., Dimitrova, R., Emmitt, G. D., Higgins, C. W., Hunt, J. C., Knierl, J. C., Lawrence, D., Liu, Y., Nadeau, D. F., Kit, E., Blomquist, B. W., Conry, P., Coppersmith, R. S., Creegan, E., Felton, M., Grachev, A., Gunawardena, N., Hang, C., Hocut, C. M., Huynh, G., Jeglum, M. E., Jensen, D., Kulandaivelu, V., Lehner, M., Leo, L. S., Liberson, D., Massey, J. D., McEnerney, K., Pal, S., Price, T., Sghiatti, M., Silver, Z., Thompson, M., Zhang, H., and Zsedrovits, T.: The MATERHORN : Unraveling the intricacies of mountain weather, *Bulletin of the American Meteorological Society*, 96, 1945–1968,
15 <https://doi.org/10.1175/BAMS-D-13-00131.1>, 2015.
- Fernando, H. J. S., Mann, J., Palma, J. M. L. M., Lundquist, J. K., Barthelmie, R. J., Belo-Pereira, M., Brown, W. O. J., Chow, F. K., Gerz, T., Hocut, C. M., Klein, P. M., Leo, L. S., Matos, J. C., Oncley, S. P., Pryor, S. C., Bariteau, L., Bell, T. M., Bodini, N., Carney, M. B., Courtney, M. S., Creegan, E. D., Dimitrova, R., Gomes, S., Hagen, M., Hyde, J. O., Kigle, S., Krishnamurthy, R., Lopes, J. C., Mazzaro, L., Neher, J. M. T., Menke, R., Murphy, P., Oswald, L., Otarola-Bustos, S., Pattanyus, A. K., Rodrigues, C. V., Schady, A., Sirin, N.,
20 Spuler, S., Svensson, E., Tomaszewski, J., Turner, D. D., van Veen, L., Vasiljević, N., Vassallo, D., Voss, S., Wildmann, N., and Wang, Y.: The Perdigão: Peering into Microscale Details of Mountain Winds, *Bulletin of the American Meteorological Society*, 100, 799–819, <https://doi.org/10.1175/bams-d-17-0227.1>, 2019.
- Foken, T.: 50 years of the Monin-Obukhov similarity theory, *Boundary-Layer Meteorology*, 119, 431–447, <https://doi.org/10.1007/s10546-006-9048-6>, 2006.
- 25 Grubišić, V., Doyle, J. D., Kuettner, J., Mobbs, S., Smith, R. B., Whiteman, C. D., Dirks, R., Czyzyk, S., Cohn, S. A., Vosper, S., Weissmann, M., Haimov, S., De Wekker, S. F. J., Pan, L. L., and Chow, F. K.: THE TERRAIN-INDUCED ROTOR EXPERIMENT, *Bulletin of the American Meteorological Society*, 89, 1513–1534, <https://doi.org/10.1175/2008BAMS2487.1>, 2008.
- Hahmann, A. N., Sile, T., Witha, B., Davis, N. N., Dörenkämper, M., Ezber, Y., García-Bustamante, E., González-Rouco, J. F., Navarro, J., Olsen, B. T., and Söderberg, S.: The making of the New European Wind Atlas – Part 1: Model sensitivity, *Geoscientific Model
30 Development*, 13, 5053–5078, <https://doi.org/10.5194/gmd-13-5053-2020>, 2020.
- Haid, M., Gohm, A., Umek, L., Ward, H. C., Muschinski, T., Lehner, L., and Rotach, M. W.: Foehn–cold pool interactions in the Inn Valley during PIANO IOP2, *Quarterly Journal of the Royal Meteorological Society*, 146, 1232–1263, <https://doi.org/10.1002/qj.3735>, 2020.
- Haupt, S. E., Kosovic, B., Shaw, W., Berg, L. K., Churchfield, M., Cline, J., Draxl, C., Ennis, B., Koo, E., Kotamarthi, R., Mazzaro, L., Mirocha, J., Moriarty, P., Muñoz-Esparza, D., Quon, E., Rai, R. K., Robinson, M., and Sever, G.: On bridging a modeling scale gap: Mesoscale to microscale coupling for wind energy, *Bulletin of the American Meteorological Society*, 100, 2533–2549,
35 <https://doi.org/10.1175/BAMS-D-18-0033.1>, 2019.
- Houghton, D. D. and Kasahara, A.: Nonlinear shallow fluid flow over an isolated ridge, *Communications on Pure and Applied Mathematics*, 21, 1–23, <https://doi.org/10.1002/cpa.3160210103>, 1968.

- Jiménez, M. A., Cuxart, J., and Martínez-Villagrasa, D.: Influence of a valley exit jet on the nocturnal atmospheric boundary layer at the foothills of the Pyrenees, *Quarterly Journal of the Royal Meteorological Society*, 145, 356–375, <https://doi.org/10.1002/qj.3437>, 2019.
- Jiménez, P. A., González-Rouco, J. F., Montávez, J. P., García-Bustamante, E., Navarro, J., and Dudhia, J.: Analysis of the long-term surface wind variability over complex terrain using a high spatial resolution WRF simulation, *Climate Dynamics*, 40, 1643–1656, <https://doi.org/10.1007/s00382-012-1326-z>, 2013.
- 5 Kaimal, J. C. and Finnigan, J. J.: *Atmospheric boundary layer flows: their structure and measurement*, Oxford University Press, New York, 1994.
- Kilpatrick, R., Hangan, H., Siddiqui, K., Parvu, D., Lange, J., Mann, J., and Berg, J.: Effect of Reynolds number and inflow parameters on mean and turbulent flow over complex topography, *Wind Energy Science*, 1, 237–254, <https://doi.org/10.5194/wes-1-237-2016>, 2016.
- 10 Lange, J., Mann, J., Angelou, N., Berg, J., Sjöholm, M., and Mikkelsen, T.: Variations of the Wake Height over the Bolund Escarpment Measured by a Scanning Lidar, *Boundary-Layer Meteorology*, 159, 147–159, <https://doi.org/10.1007/s10546-015-0107-8>, 2016.
- Lange, J., Mann, J., Berg, J., Parvu, D., Kilpatrick, R., Costache, A., Chowdhury, J., Siddiqui, K., and Hangan, H.: For wind turbines in complex terrain, the devil is in the detail, *Environmental Research Letters*, 12, 094 020, <https://doi.org/10.1088/1748-9326/aa81db>, 2017.
- Lehner, M., Whiteman, C. D., Hoch, S. W., Crossman, E. T., Jeglum, M. E., Cherukuru, N. W., Calhoun, R., Adler, B., Kalthoff, N., Rotunno, R., Horst, T. W., Semmmer, S., Brown, W. O., Oncley, S. P., Vogt, R., Grudzielanek, A. M., Cermak, J., Fonteyne, N. J., Bernhofer, C., Pitacco, A., and Klein, P.: The METCRAX II Field Experiment: A Study of Downslope Windstorm-Type Flows in Arizona’s Meteor Crater, *Bulletin of the American Meteorological Society*, 97, 217–235, <https://doi.org/10.1175/BAMS-D-14-00238.1>, 2016.
- 15 Long, R. R.: Some Aspects of the Flow of Stratified Fluids: II. Experiments with a Two-Fluid System, *Tellus*, 6, 97–115, <https://doi.org/10.3402/tellusa.v6i2.8731>, 1954.
- 20 Mann, J., Angelou, N., Arnqvist, J., Callies, D., Cantero, E., Arroyo, R. C., Courtney, M., Cuxart, J., Dellwik, E., Gottschall, J., Ivanell, S., Kühn, P., Lea, G., Matos, J. C., Palma, J. M. L. M., Pauscher, L., Peña, A., Rodrigo, J. S., Söderberg, S., Vasiljevic, N., and Rodrigues, C. V.: Complex terrain experiments in the New European Wind Atlas, *Philosophical Transactions of the Royal Society A: Mathematical, Physical and Engineering Sciences*, 375, 20160 101, <https://doi.org/10.1098/rsta.2016.0101>, 2017.
- Martínez, D., Jiménez, M. A., Cuxart, J., and Mahrt, L.: Heterogeneous nocturnal cooling in a large basin under very stable conditions, *Bound.-Layer Meteor.*, 137, 97–113, <https://doi.org/http://dx.doi.org/10.1007/s10546-010-9522-z>, 2010.
- 25 Menke, R., Vasiljevi, N., Mann, J., and Lundquist, J. K.: Characterization of flow recirculation zones at the Perdigão site using multi-lidar measurements, *Atmospheric Chemistry and Physics*, 19, 2713–2723, <https://doi.org/10.5194/acp-19-2713-2019>, 2019.
- Olsen, B. T., Hahmann, A. N., Sempreviva, A. M., Badger, J., and Jørgensen, H. E.: An intercomparison of mesoscale models at simple sites for wind energy applications, *Wind Energy Science*, 2, 211–228, <https://doi.org/10.5194/wes-2-211-2017>, 2017.
- 30 Palma, J. M., Silva Lopes, A., Costa Gomes, V. M., Veiga Rodrigues, C., Menke, R., Vasiljević, N., and Mann, J.: Unravelling the wind flow over highly complex regions through computational modeling and two-dimensional lidar scanning, *Journal of Physics: Conference Series*, 1222, <https://doi.org/10.1088/1742-6596/1222/1/012006>, 2019.
- Pauscher, L., Vasiljevic, N., Callies, D., Lea, G., Mann, J., Klaas, T., Hieronimus, J., Gottschall, J., Schwesig, A., Kühn, M., and Courtney, M.: An Inter-Comparison Study of Multi- and DBS Lidar Measurements in Complex Terrain, *Remote Sensing*, 8, 782, <https://doi.org/10.3390/rs8090782>, 2016.
- 35 Rotunno, R. and Bryan, G. H.: Numerical Simulations of Two-Layer Flow past Topography. Part I: The Leaside Hydraulic Jump, *Journal of the Atmospheric Sciences*, 75, 1231–1241, <https://doi.org/10.1175/jas-d-17-0306.1>, 2018.

- Rotunno, R. and Lehner, M.: Two-Layer Stratified Flow past a Valley, *Journal of the Atmospheric Sciences*, 73, 4065–4076, <https://doi.org/10.1175/jas-d-16-0132.1>, 2016.
- Salmon, J. R., Bowen, A. J., Hoff, A. M., Johnson, R., Mickle, R. E., Taylor, P. A., Tetzlaff, G., and Walmsley, J. L.: The Askervein Hill Project: Mean wind variations at fixed heights above ground, *Boundary-Layer Meteorology*, 43, 247–271, <https://doi.org/10.1007/BF00128406>, 1988.
- 5 Santos, P., Mann, J., Vasiljevic, N., Courtney, M., Sanz Rodrigo, J., Cantero, E., Borbón, F., Martínez-Villagrasa, D., Martí, B., and Cuxart, J.: The Alaiz Experiment (ALEX17): wind field and turbulent fluxes in a large-scale and complex topography with synoptic forcing, <https://doi.org/10.11583/DTU.c.4508597.v1>, 2019.
- Sanz Rodrigo, J., Borbón Guillén, F., Gómez Arranz, P., Courtney, M. S., Wagner, R., and Dupont, E.: Multi-site testing and evaluation of remote sensing instruments for wind energy applications, *Renewable Energy*, 53, 200–210, <https://doi.org/10.1016/j.renene.2012.11.020>, 2013.
- 10 Sanz Rodrigo, J., Chávez Arroyo, R. A., Moriarty, P., Churchfield, M., Kosović, B., Réthoré, P. E., Hansen, K. S., Hahmann, A., Mirocha, J. D., and Rife, D.: Mesoscale to microscale wind farm flow modeling and evaluation, *Wiley Interdisciplinary Reviews: Energy and Environment*, 6, <https://doi.org/10.1002/wene.214>, 2017.
- 15 Serafin, S., Adler, B., Cuxart, J., De Wekker, S. F., Gohm, A., Grisogono, B., Kalthoff, N., Kirshbaum, D. J., Rotach, M. W., Schmidli, J., Stiperski, I., Večenaj, Ž., and Zardi, D.: Exchange processes in the atmospheric boundary layer over mountainous terrain, *Atmosphere*, 9, 1–32, <https://doi.org/10.3390/atmos9030102>, 2018.
- Simó, G., Cuxart, J., Jiménez, M. A., Martínez-Villagrasa, D., Picos, R., López-Grifol, A., and Martí, B.: Observed Atmospheric and Surface Variability on Heterogeneous Terrain at the Hectometer Scale and Related Advective Transports, *Journal of Geophysical Research: Atmospheres*, 124, 9407–9422, <https://doi.org/10.1029/2018JD030164>, 2019.
- 20 Strauss, L., Serafin, S., and Grubišić, V.: Atmospheric Rotors and Severe Turbulence in a Long Deep Valley, *Journal of the Atmospheric Sciences*, 73, 1481–1506, <https://doi.org/10.1175/JAS-D-15-0192.1>, 2016.
- Vasiljević, N., Lea, G., Courtney, M., Cariou, J. P., Mann, J., and Mikkelsen, T.: Long-range WindScanner system, *Remote Sensing*, 8, 1–24, <https://doi.org/10.3390/rs8110896>, 2016.
- 25 Vasiljević, N., Palma, J. M., Angelou, N., Matos, J. C., Menke, R., Lea, G., Mann, J., Courtney, M., Frölen Ribeiro, L., and Gomes, V. M.: Perdigoão 2015: Methodology for atmospheric multi-Doppler lidar experiments, *Atmospheric Measurement Techniques*, 10, 3463–3483, <https://doi.org/10.5194/amt-10-3463-2017>, 2017.
- Vosper, S. B.: Inversion effects on mountain lee waves, *Quarterly Journal of the Royal Meteorological Society*, 130, 1723–1748, <https://doi.org/10.1256/qj.03.63>, 2004.
- 30 Walmsley, J. L. and Taylor, P. A.: Boundary-layer flow over topography: Impacts of the Askervein study, *Boundary-Layer Meteorology*, 78, 291–320, <https://doi.org/10.1007/BF00120939>, 1996.
- Whiteman, C. D., Lehner, M., Hoch, S. W., Adler, B., Kalthoff, N., and Haiden, T.: Katabatically driven cold air intrusions into a basin atmosphere, *Journal of Applied Meteorology and Climatology*, 57, 435–455, <https://doi.org/10.1175/JAMC-D-17-0131.1>, 2018.
- Wilczak, J. M., Stoelinga, M., Berg, L. K., Sharp, J., Draxl, C., McCaffrey, K., Banta, R. M., Bianco, L., Djalalova, I., Lundquist, J. K., 35 Muradyan, P., Choukulkar, A., and Le, A. B.: The Second Wind Forecast Improvement Project (WFIP2): Observational Field Campaign, *Bulletin of the American Meteorological Society*, 100, 1701–1723, <https://doi.org/10.1175/BAMS-D-18-0035.1>, 2019.
- Wyngaard, J. C.: Toward numerical modeling in the "Terra Incognita", *Journal of the Atmospheric Sciences*, 61, 1816–1826, [https://doi.org/10.1175/1520-0469\(2004\)061<1816:TNMITT>2.0.CO;2](https://doi.org/10.1175/1520-0469(2004)061<1816:TNMITT>2.0.CO;2), 2004.